Fall 2019

Sediment Resuspension in a Microtidal Estuary: Causative Forces and Links with Algal Blooms

Samantha C. McGill
Old Dominion University, scmcgill79@gmail.com

SEDIMENT RESUSPENSION IN A MICROTIDAL ESTUARY:

CAUSATIVE FORCES AND LINKS WITH ALGAL BLOOMS

by

Samantha C. McGill
B.S. May 2013, Coastal Carolina University

A Thesis Submitted to the Faculty of
Old Dominion University in Partial Fulfillment of the
Requirements for the Degree of

MASTER OF SCIENCE

OCEAN AND EARTH SCIENCE

OLD DOMINION UNIVERSITY
December 2019

Approved by:

Richard P. Hale (Director)

Margaret R. Mulholland (Member)

Tal Ezer (Member)

ABSTRACT

SEDIMENT RESUSPENSION IN A MICROTIDAL ESTUARY: CAUSATIVE FORCES AND LINKS WITH ALGAL BLOOMS

Samantha C. McGill
Old Dominion University, 2019
Director: Dr. Richard P. Hale

After years of efforts to restore the Chesapeake Bay, bacterial levels are down and species diversity has increased, however, algal blooms (primarily dinoflagellates) persist, occurring nearly every summer. Dinoflagellates produce resting cysts that accumulate in the bottom sediments and are thought to provide seed populations for future algal blooms when they are resuspended. When estuarine sediments are advected from a bed, other materials, such as pollutants, nutrients, and organic matter are also released into the water column. Thus, resuspended sediments can contribute to the degradation of water quality, habitat, and aquatic life, and impart negative impacts on local ecosystems and economies. To investigate the causes of sediment resuspension in a shallow, tidal system and the potential role of sediment resuspension on algal production, time-series measurements of current velocity, wave height, and suspended sediment concentrations were recorded using acoustic, optical, and pressure sensors, in conjunction with a temporal and spatial survey of conductivity, temperature, suspended sediment concentration profiles, benthic sediment samples, and water samples. Regional meteorological data including hourly wind speed and direction and precipitation totals were also compiled for comparison with sediment resuspension, chlorophyll *a* (Chl *a*) concentrations and dissolved nutrient concentrations. Sediment resuspension in estuaries typically results from wind-driven waves, tidal currents, or wind-driven currents. Results from this study found maximum wave orbital velocities (U_{bm}) to be an order of magnitude less than current velocities

(U_c), however, periods of elevated $U_{bm,}$ were associated with the majority of observed resuspension events. Despite surface gravity waves primarily causing resuspension, currents (tidal and wind-driven), as well as water depth, appeared to mitigate or even negate wave induced resuspension. Overall, resuspension most often resulted when U_{bm} >~2 cm/s, coinciding with southwesterly winds ≥ 5 m/s, during periods of relatively weak current speeds and water depth. Observation of increased nutrient concentrations and/or Chl *a* concentrations followed numerous resuspension events, suggesting that resuspension likely aided in the growth of algal blooms observed in the Lafayette River. The link between sediment resuspension, elevated nutrient and Chl *a* concentrations, was supported via observations of elevated near-bed concentrations of ammonium and nitrate/nitrite concentrations. Nutrient concentrations in bottom waters then declined as Chl *a* concentrations increased. The timing of this sequence of events (2-7 days) was on the order observed previously. This study suggests that sediment resuspension may be an import factor for stimulating algal production in shallow, eutrophic, microtidal estuaries.

This thesis is dedicated first and foremost to my parents for their endless support and second to the person(s) who changed the trajectory of my path unknowingly for the better.

ACKNOWLEDGMENTS

There are numerous individuals who supported me throughout the course of my graduate work, in different ways and at different points in time, whom I owe many thanks to. First, I'm incredibly thankful for my advisor Dr. Richard Hale, I would not be where I am now without his unwavering support, patience, guidance, and knowledge. Additionally, I am appreciative of my committee member, Dr. Margaret Mulholland for her endless support and guidance as well. Both Drs. Hale and Mulholland provided tremendous support with this research, made time in their busy schedules to meet with me whenever I had questions, wanted their feedback or wanted to run through yet another practice talk. I'd also like to thank my committee member Dr. Tal Ezer for his guidance and knowledge through this thesis.

Additionally, I owe tremendous thanks to Dr. Gail Dodge, I would not have had this opportunity, if it weren't for her. I am also thankful for the support and guidance that I received from Dr. Fred Dobbs. Further, I am incredibly grateful for Dr. Shannon Wells, she has been a tremendous support and mentor from day one. I have learned so much from her and as a result have significantly improved my ability to teach and communicate science, due to the advice, knowledge, and support that she provided while I was a lab instructor under her supervision.

I am forever appreciative of the members of the Mulholland lab for providing me with all of their field sampling data. Specifically, I'm thankful for Lab Manager Pete Bernhardt, whom I learned numerous lab skills and techniques from, as well as Michael Echeveria for answering my endless questions and providing support with the sampling data. I also have the utmost gratitude for the rest of the sampling team: Eduardo Vega Perez, Alfonso Macias Tapia, and Iliana Flefel, for their endless hours spent in the field and the lab collecting data that made this thesis possible.

Last but not least, I am extremely grateful for the perpetual support that I received from my family, friends, and fellow graduate students. I would not have made it through these past few years if it weren't for the support that I received from all of them, for that, I am truly grateful.

TABLE OF CONTENTS

LIST OF TABLES

LIST OF FIGURES

Figure Page

Figure Page

CHAPTER 1

INTRODUCTION

In estuarine environments, most sediments are supplied via upstream fluvial systems, surface runoff, bank erosion, and resuspension via advection from waves and currents (Webster and Lemckert, 2002). Resuspension returns sediment that has been temporarily deposited, back into the transportation system for removal and delivery to its ultimate depocenter (Nichols, 1992). In eutrophic estuaries such as the lower Chesapeake Bay, resuspension can also introduce dissolved nitrogen (N) and phosphorus (P) regenerated from organically enriched sediments, into the water column. Sediment resuspension occurs when bed shear stress exceeds the combined forces of particle settling velocity and friction between particles and the bed, where shear stress predominantly results from surface gravity waves generated by winds (Booth et al., 2000) or from currents which may be tidal, wind-driven, or density-driven (Allen, 1974; Green and Coco, 2013). However, in microtidal environments, such as the Lafayette River, a sub-estuary of the lower Chesapeake Bay, wind-generated waves often act as the primary force responsible for sediment resuspension (Booth et al., 2000; Carniello et al., 2005; Fagherazzi et al., 2007).

Suspended and resuspended sediments can have deleterious effects on ecosystems and economies. These include the loss of wetlands and shorelines (Brand et al., 2010), infilling of channels or changes to bathymetry (Nichols, 1992; Webster and Lemckert, 2002), mortality of benthic organisms (Rossi et al., 2012; U.S. Environmental Protection Agency, 1996), increased light attenuation and consequential decreases in primary production (Najjar et al., 2010; Schallenberg and Burns, 2004), as well as the reintroduction of noxious materials and toxins into the water column (Gartner, 2004; Nichols, 1992; Rossi et al., 2012). In addition to these potentially harmful substances, bottom sediments often contain nutrients (Simon, 1989; Arfi et

al., 1993; Corbett, 2010) that have been regenerated from the degradation of accumulated organic matter, as well as algal cysts which can be deposited to the sediments when certain types of algae are abundant. Both nutrients (Tang et al., 2010; Morse et al., 2011, 2014; Shin et al., 2017) and cysts (Tang and Gobbler, 2012; Nehring, 1996; Mohamed and Al-Shehri, 2011; Keafer et al., 1992; He et al., 2008; McGillicuddy et al., 2011; Butman et al., 2014) are essential components in the formation of certain algal blooms (e.g., dinoflagellates), which also may lead to the degradation of water quality.

Algal cysts are formed by many dinoflagellate species as part of their life cycle, during reproduction, or when exposed to environmental stressors; and are typically found in surface or subsurface sediments of water bodies where blooms previously occurred (Nehring, 1996; Tang and Gobbler, 2012; Shin et al., 2017). Cysts located in the superficial or subsuperficial sediments are thought to be the "seed" population for future blooms (Nehring, 1996) and have been shown in models to be a first-order predictor of bloom severity (He et al., 2008; McGillicuddy et al., 2011; Butman et al., 2014). While the triggers for germination of dinoflagellate cysts, are not completely understood and vary among species; numerous studies on the germination of cysts have shown the complete inhibition of excystment for a variety of dinoflagellate species when in anoxic conditions (Anderson et al., 1987; Nehring, 1996; Kremp and Anderson, 2000). As such, cysts that are buried in anoxic sediments are not considered part of the population pool, unless a mechanism such as bioturbation or sediment resuspension can return them to aerobic conditions (Nehring, 1996). Sediment resuspension has been shown to impact bloom formation by advecting cysts into water column where light-assisted germination can occur (Anderson et al., 1987; Butman et al., 2014; Kremp, 2001), and by supplying nutrients necessary for algal growth (Tang and Gobbler, 2012; Shin et al., 2017).

Cysts of dinoflagellate species can be found throughout sediments of the lower Chesapeake Bay and many of its tributaries (Seaborn and Marshall, 2008). Cysts of *Margalefidinium polykrikoides,* formerly *Cochlodinium polykrikoides*, are of particular interest and concern given the species' known capacity to form massive blooms (Seaborn and Marshall, 2008; Mulholland et al., 2009). *M. polykrikoides* is often referred to as a "mahogany tide", due to the reddish hue it imparts on the water when these organisms are present in elevated amounts. It is also considered a "harmful algae" due to its ability to have lethal effects on larval and juvenile fish and oysters (Gobbler et al., 2008; Mulholland et al., 2009;). In addition to having lethal properties, the dense blooms formed by *M. polykrikoides* can generate hypoxic conditions during bloom degradation, which can also result in the mortality of aquatic organisms (Smayda, 1997a; Tango et al., 2005). The impacts of *M. polykrikoides* are not limited to the Chesapeake Bay region, as blooms of this species have been documented in mid and low-latitude water bodies around the world. Catastrophic blooms of *M. polykrikoides* have been observed in the Caribbean Sea, eastern and western Pacific Ocean, the western Atlantic Ocean, Indian Ocean, Mediterranean Sea, Arabian Gulf, Korea's Masan Bay, and Lampung Bay in Sumatra (Margalef, 1961; Matsuoka et al., 2008; Mohamed and Al-Shehri, 2011; Tang and Gobbler, 2012; Jeong et al., 2013; Thoah et al., 2019).

The spatial extent and severity of *M. polykrikoides* blooms have led to numerous investigations that have related an array of complex factors associated with bloom development and initiation, among which include nutrient stimulation (Tang et al., 2010; Tang and Gobbler, 2012; Morse et al., 2014; Shin et al., 2017). In the Lower Chesapeake Bay, the formation and extent of *M. polykrikoides* blooms have been associated with intense rainfall events, and accompanying nutrient loading (Mulholland et al., 2009; Morse et al., 2011); spring-neap tidal

modulation, increased stratification, and estuarine mixing (Morse et al., 2011). Further, a hotspot linked to bloom initiation has been identified in the Lafayette River, a shallow sub-estuary of the Chesapeake Bay (Morse et al., 2011). The Lafayette River is a shallow micro-tidal estuary, that connects to the Elizabeth River and lower James River near their confluence with the Chesapeake Bay (Fig. 1; Blair et al., 1976; Berman et al., 2002; Egerton et al., 2014). Blooms initiating in the Lafayette River have been shown to spread into the Elizabeth River and lower James River via tidal flushing and estuarine circulation (Morse et al., 2011). Despite a general understanding of the various factors associated with bloom initiation and transport, predicting their occurrence continues to prove extremely challenging. Further, the relationship between sediment resuspension and bloom initiation has not been examined at these bloom initiation hotspots. Therefore, in this study, I examine sediment resuspension and its potential impacts on bloom formation in the Lafayette River.

Based on field data, local observations, and available literature, I hypothesized that sediment resuspension resulting from a combination of wind-driven surface gravity waves and tidal currents, aids in the formation and proliferation of harmful dinoflagellate blooms through advection of cysts and nutrients. A multi-faceted approach was necessary to understand sediment resuspension and its link to dinoflagellate blooms. In this study, I combined observations and measurements of sediment resuspension and its causative mechanisms, with detailed bloom monitoring data. These measurements were recorded by of a variety of sensors deployed at a monitoring station, near the terminal head of the Lafayette River. Time-series observations of backscatter intensities, current speeds, and estimated wave orbital velocities, were analyzed against concurrent meteorological observations and tidal phases. Hydrodynamic and meteorological conditions were then compared with a combination of sonde measurements and

water samples collected at multiple depths, carried out by the Mulholland Lab at Old Dominion University. These included Chl *a* concentrations, cell counts, and dissolved concentrations of a variety of nutrients including nitrate+nitrite, phosphate, and ammonium. These data were used to identify and verify the presence of dinoflagellate blooms and were analyzed for auto-correlation and cross-correlation with nutrient concentrations as well as resuspension events.

While no previous research has focused on the role of sediment resuspension in bloom formation and propagation in the lower Chesapeake Bay region, a modelling study in the Gulf of Maine suggests that resuspension and subsequent transport of sediment and cysts were important factors for predicting *Alexandrium fundyense* blooms as resuspension may transport cysts into the water column where germination is facilitated (Butman et al., 2014). In the Baltic Sea, sediment resuspension aided in the germination of some species but not others, influence species composition (Kremp, 2001). In Kremp's study *Scrippsilla hangoei* cysts were resuspended by strong storms, allowing light to significantly increase germination frequency, while the percentage of *Peridiniella catenata* excystment was not significantly influenced (2001).

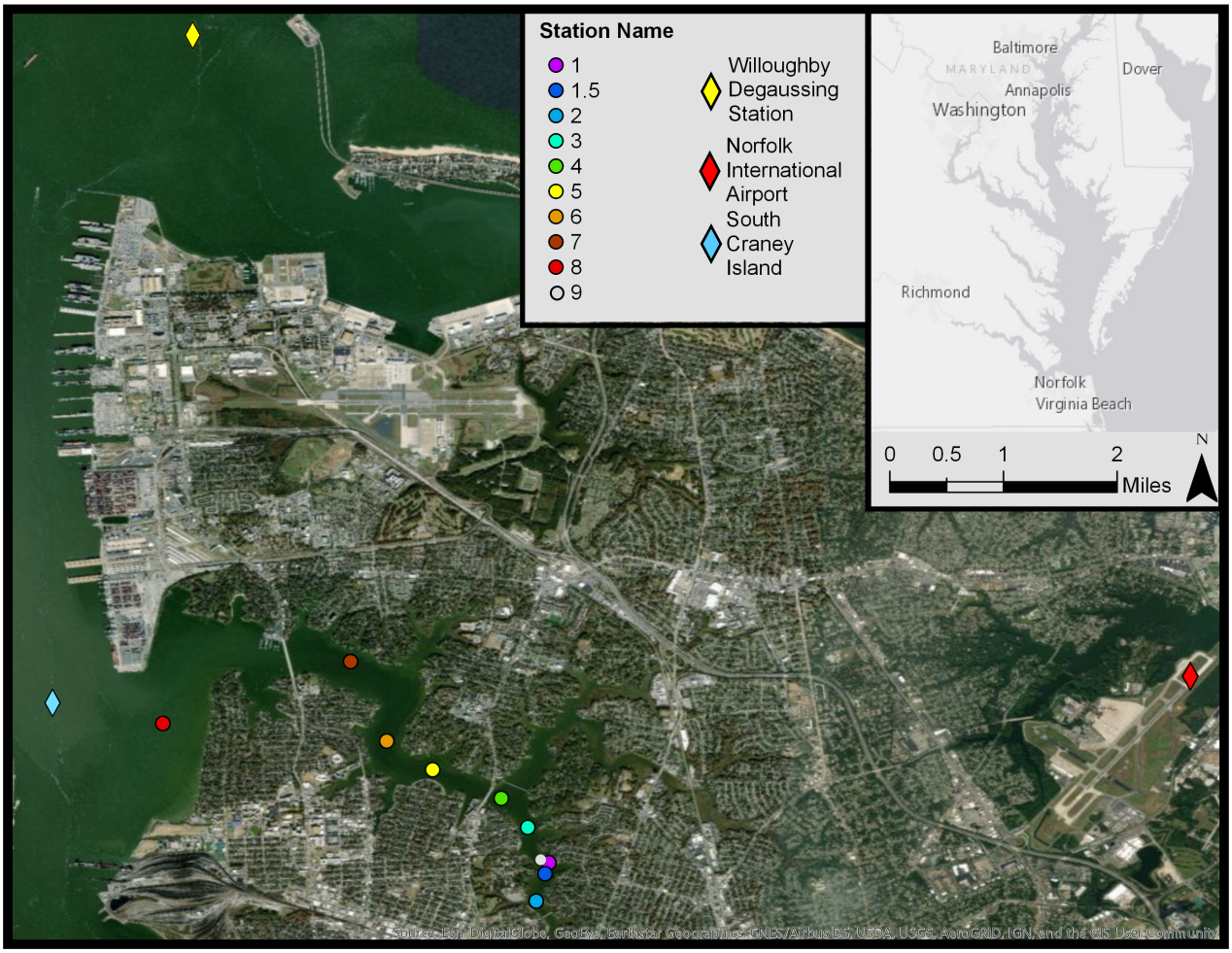

Figure 1. The Lafayette River estuary is located in Southeastern Virginia. Stations where water samples and CTD casts were done are noted on the map as circles or triangles. Station 9 was the initial location of the ADCP, which was later moved to station 1. Meteorological data were collected from Norfolk International Airport, as well as South Craney Island.

CHAPTER 2

METHODS

STUDY SITE

The Ashland Circle (AC) monitoring site is located near the head of the Lafayette River estuary in Norfolk, Virginia (Fig. 1). This monitoring site has been maintained since 2015 by the Mulholland lab at Old Dominion University and was chosen as the primary location for field measurements, due to the existence of historical and ongoing hydrographic records, its relatively long fetch nearly aligning with the direction of local prevailing winds, and observations suggesting that blooms initiate in this area. The Lafayette River has a mean depth of 1.2 m below mean low water (MLW) (Egerton et al., 2014; Blair et al., 1976), with a maximum channel depth ranging from 2-6 m (Blair et al., 1976). AC has an average depth of approximately 2 meters. The estuary shoals from mouth to head, with its deepest waters located near its confluence with Elizabeth River and in its dredged channel that extends to the primary bifurcation in the river, approximately 5 km inland from the mouth.

SENSOR DEPLOYMENTS

Time-series data were collected during six deployments between January 26th and October 2nd 2018. Sensors included a pulse-coherent acoustic Doppler current profiler (ADCP), mounted on a frame with two optical backscatter sensors (OBS), and a high-frequency conductivity, temperature, and depth sensor (CTD). The first deployment (1/26/2018- 2/19/2018) at the Ashland Circle station was too shallow, exposing the top OBS at times, so all subsequent deployments occurred ~110 m southeast of the first site, where the average water depth was deeper (2 meters).

For each deployment, the ADCP was secured to a weighted frame, such that the pressure sensor was at approximately 15 cm above bed (cmab), and the acoustic sensors were roughly 19 cmab (Fig. 2). Between each deployment the ADCP was cleaned, repowered, and applied with a new coating of zinc oxide (used as an antifoulant). The ADCP has three upward-facing acoustic sensors that transmit 1-MHz sound pulses into the water column, where they are scattered and reflected by suspended particles. Moving water results in a frequency shift in the returned signal, known as the Doppler shift, which is used to calculate velocity profiles in 3-cm bins that extend from ~60 cmab to the water surface. Water depth was measured by a high-resolution pressure sensor within the ADCP. Measurements were collected in bursts at a rate of 1 Hz for 256 seconds at 60-minute intervals. The data recorded by the ADCP were burst averaged, range corrected, and adjusted for surface and bottom boundary offsets via routines that were run using the MathWorks' MATLAB software. In addition to the velocity profiles and water depth, the acoustic backscatter intensity was used as a proxy for suspended sediments. Near-bed current velocity (U_{cb}) and backscatter were calculated by averaging bins 2 through 11, corresponding to ~60-90 cmab, while the mean (or depth averaged) current speed (U_c) was the average of bins 2 through 51. The first and last bins were excluded from these calculations as they were presumed to contain the most noise.

Two optical backscatter sensors were deployed with the ADCP, at elevations of ~0.5 and 50 cmab (Fig. 2). After the initial deployment, the sensors were treated with a one-time application of an antifouling agent to minimize impairment from biofouling. OBS emit infrared light that reflects upon contact with particles, with the instrument recording the intensity of this reflection. As with velocity measurements, data were burst averaged to filter any high-frequency noise. The filtered data were converted to suspended sediment concentrations (SSC) using a

calibration curve from based on lab measurements, following a method described by Ogston and Sternberg (1999). In the lab, sediment from the study site, was incrementally added to a large volume of water that was continuously mixed. After each addition of sediment, water samples were collected using a pipette, the while OBS measurements were recorded. These water sample volumes were recorded, then vacuum drawn onto pre-weighed 0.7-µm glass-fiber filters, which were dried in an oven at ~50 ºC and re-weighed, with the difference in weights used to calculate SSC. The SSC were plotted against the recordings from both OBS, where the slopes for each sensor were used to convert instrument response to SSC. Calibrations curves of the OBS' showed linear relationships between SSC and OBS intensity for both the top (R^2=0.995) and bottom sensor (R^2=0.99; Fig. 3). Given the improved sensitivity of the OBS relative to acoustic backscatter, as well as the location of an OBS sensor completely within the wave boundary layer, resuspension events were determined with OBS data.

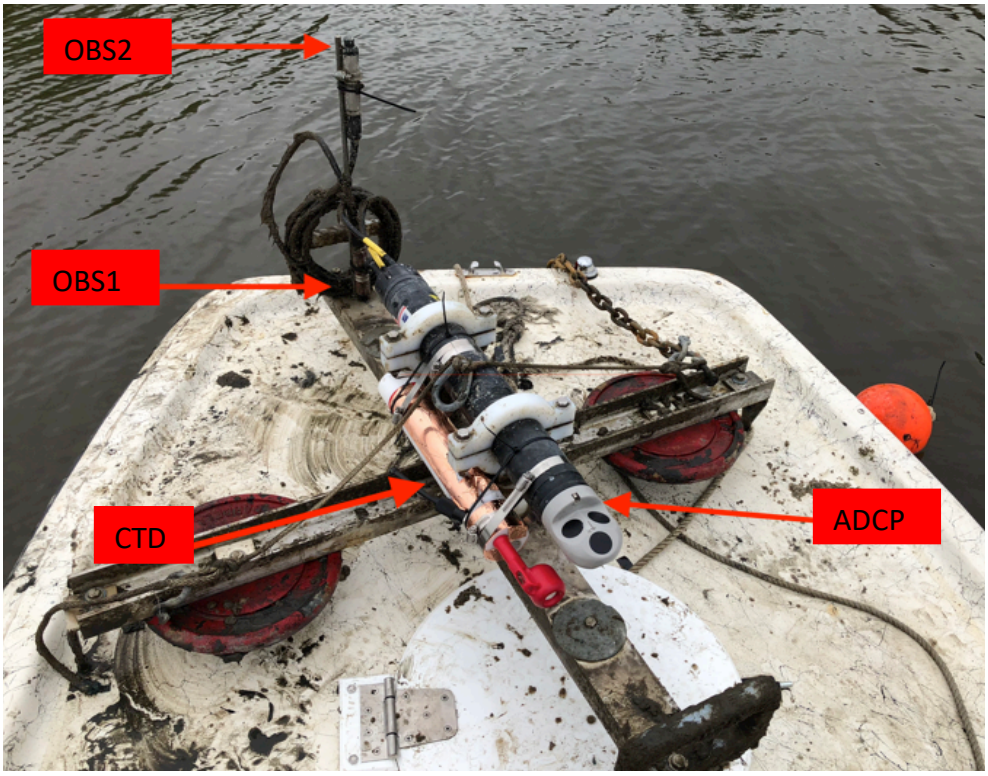

Figure 2. Image of the ADCP mounted on the frame with the CTD and both OBS immediately prior to redeployment.

Deployments 3 (5/7/18-6/6/18) and 6 (9/11/18-10/2/18) included a CTD with a sampling frequency of 6 Hz. The pressure data recorded by the CTD were used to estimate non-directional spectral and zero-crossing wave parameters using MATLAB routines created by Urs Neumeier (2003) after being detrended and corrected for depth attenuation and sea-surface pressure. Frequency cutoffs were to set 1 and 0.05 Hz, which correspond to periods of 1 and 20 seconds, respectively, for calculating wave parameters from the power spectral density. These cutoffs filtered out fluctuations that were not directly related to the orbital motion of the waves (Elfrink et al., 2006). The near bed maximum wave orbital velocity was calculated using the transitional water depth equations from the Shoreline Protection Manual (1984). An additional CTD, with

an incorporated OBS sensor, was used to measure water-column properties during casts at the various stations (Fig. 1) to characterize hydrographic spatial variability.

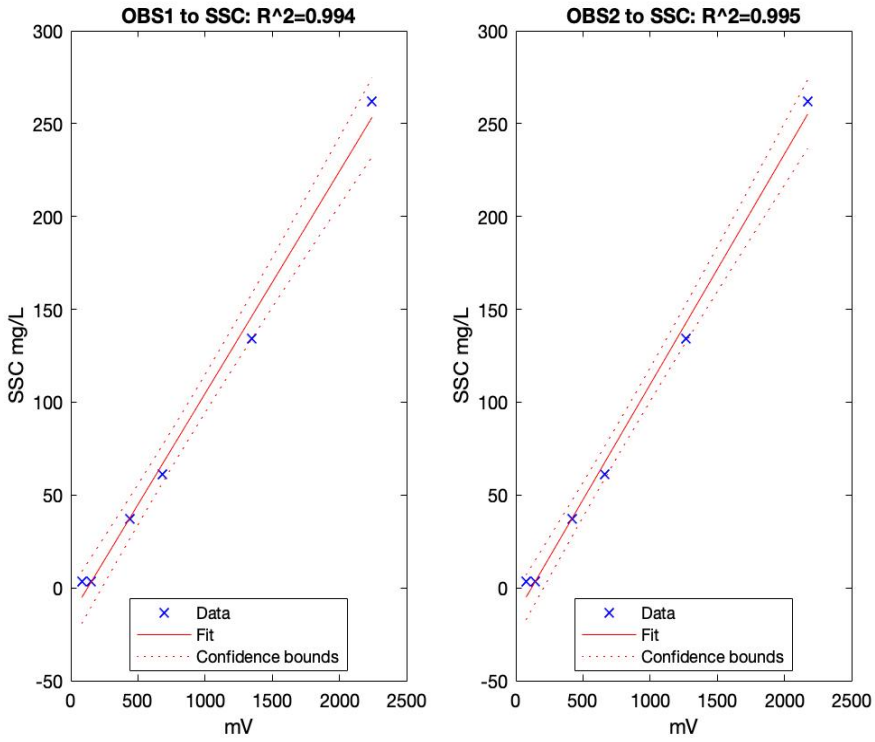

Figure 3. Calibration curves for the bottom OBS (left graph) and top OBS sensor (right graph), used to estimate the suspended sediment concentrations from OBS intensity.

SEDIMENT AND WATER SAMPLES

Sediment samples were collected using a Ponar sediment grab during the first, third, and fourth deployments at Ashland Circle and at all stations at the start of deployment 4 (Fig. 4). Samples were placed in bags and chilled until subsequent analysis, using a Malvern Mastersizer 1000 particle-size analyzer. The Malvern determines the particle size distribution by measuring the angular variation of scattered light intensity as a laser beam passes through a dispersed particulate sample (Malvern Panalytical, 2018). The sediment grab samples were prepared by

measuring out ~1 gram of sediment sample, adding 7 drops of sodium hexametaphosphate used as a dispersing agent, diluting with 40 mL of deionized water, and allowing to soak for a minimum of 24 hours. Samples were sonified for 2 minutes and immediately pipetted into the Malvern for analysis. D_{50} values from the results of the particle size analysis provided the median diameter of the sample where 50% of the sample is larger and 50% of the sample is smaller. These D_{50} values are used to reference grain size throughout this study.

Surface water samples were collected using 500-ml bottles from the side of the boat to measure surface SSC. Sample volumes were measured and then vacuum drawn onto pre-weighed 0.7-µm glass-fiber filters, which were weighed and dried in an oven at ~50 ºC. Following equation 1, SSC was calculated in units of milligrams per liter, where filter weights were in units of milligrams, and sample volume was in units of liters.

$$\frac{(post\ filter\ weight - pre\ filter\ weight)}{Total\ sample\ Volume} = SSC \quad (1)$$

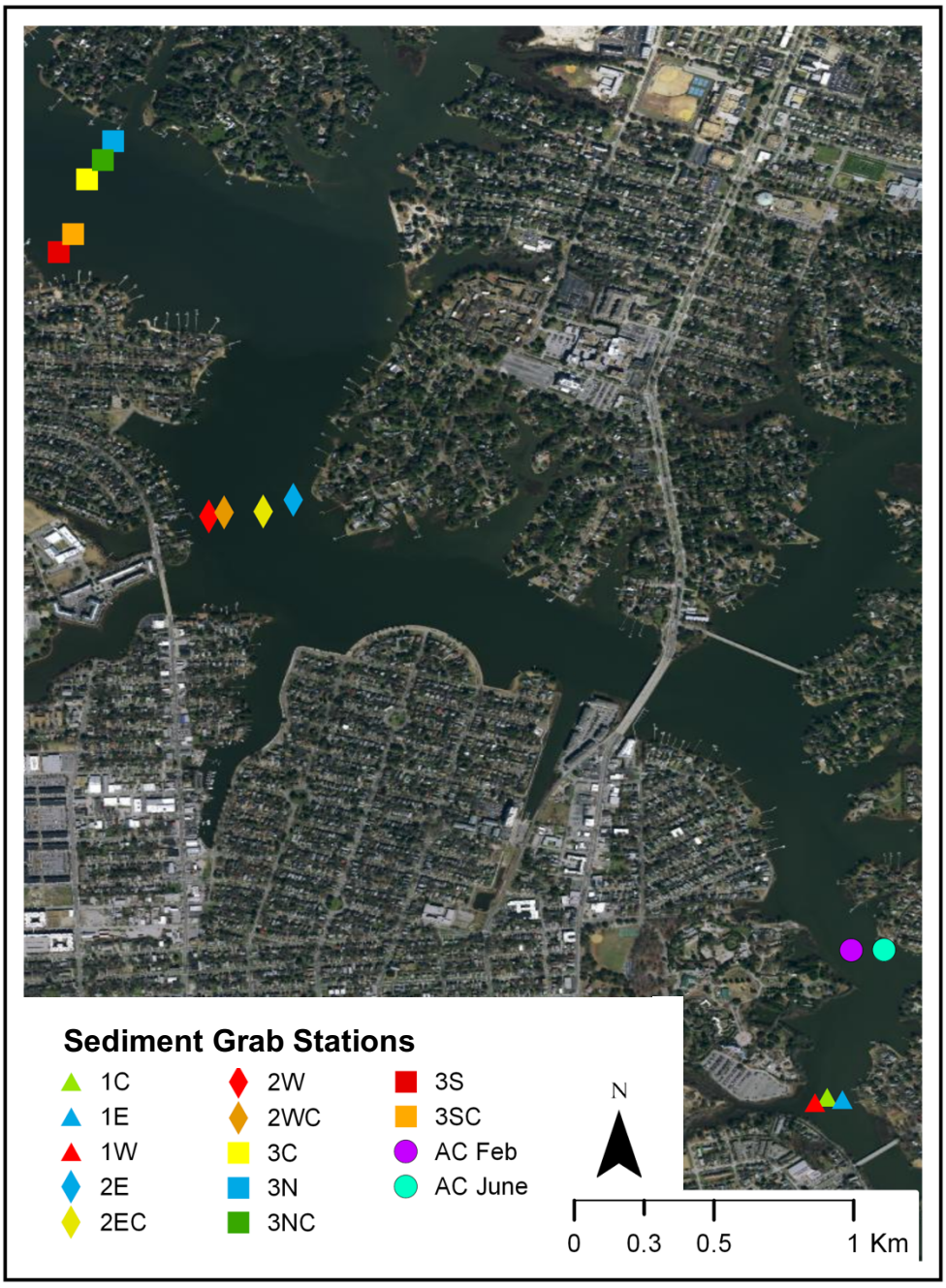

Figure 4. Stations where sediment grabs were collected during the 4th deployment in addition to at Ashland Circle sites during February and June.

Deployment:	1	2	3	4	5	6
Dates	1/26-2/19	4/2-5/7	5/7-6/6	6/6-7/20	7/20-9/6	9/11-10/2
ADCP	X	X	X	X	X	X
OBS	X	X	X	X	X	X
CTD			X			X
Water Sample(s)			X	X	X	X
Sediment	X		X			
CTD profiles			X	X	X	X

Table 1. A breakdown of the data collected/ instruments used for each deployment.

BLOOM MONITORING

Additional hydrographic data collected at AC were provided by the Mulholland Lab at Old Dominion University. These data included bi-weekly sonde profiling and multi-depth water sampling which commenced at the end of May 2018. Beginning on June 10, 2018, sampling occurred daily due to the elevated Chl *a* concentrations and dinoflagellate abundance. Discrete measurements were accompanied by continuous measurements collected by a YSI sonde moored to a dock at AC, starting in July. The sondes measured pH, temperature, turbidity, Chl *a* fluorescence, dissolved oxygen, conductivity, and depth. Water samples collected were analyzed for ammonium, combined nitrate-nitrite, phosphate, and Chl *a*, in addition to cell abundance and species identification. The presence of a *M. polykrikoides* bloom was defined by a cell density of 1000 cell/mL. The term "bloom" was used to reference other dinoflagellate species throughout this study, where a single species was present in elevated concentrations and was significantly more abundant than other species that were present.

METEROLOGICAL DATA

Meteorological data were collected from NOAA's Tides & Currents webpage (http://tidesandcurrents.noaa.gov), and Environmental Information websites (https://www.ncdc.noaa.gov/), for 2018. These data included hourly wind speed and direction from South Craney Island Station, and daily averaged wind speed and precipitation from Norfolk International Airport. South Craney Island's station is approximately 6.4 km from Ashland Circle and Norfolk International Airport's station is approximately 7.5 km from Ashland Circle. These stations were used because of their close proximity to the study area as well as availability and completeness of data. Wind velocity data were also collected from Willoughby Degaussing Station and used for the duration of the final deployment due to unavailability of data from South Craney Island during for this period. Willoughby Degaussing Station is located roughly 12 km NNE from AC (Fig. 1).

DATA ANALYSIS

Linear regression and multiple regression techniques were used to explore the relationships between current speed, near bed maximum wave orbital velocity, water depth to wave length ratio (wave type), wind speed, acoustic backscatter, SSC, bottom nutrient concentrations (combined NO_3^- NO_2^-, NH_4^+, PO_4^{3-}), and Chl *a* concentrations. To compare data that were sampled at different frequencies, higher frequency datasets were reduced to timepoints that corresponded with intervals of the lower-frequency dataset.

A 38-hour low pass, fourth order Butterworth filter was applied to the current speed, wind, and OBS data in order to remove the presence of the semidiurnal tides and examine the data for signs of wind-driven currents.

CRITICAL WIND SPEED

The critical wind speed, (U_{wc}), (equation 3), associated with the onset of resuspension was calculated following the method used in Booth et al. (2000) and the formulations from the U.S. Army Coastal Engineering Research Center (1984). In order to use this method, the fetch (F) associated with each wind direction observed had to be determined. To do this, wind directions were binned in 12-degree increments, the fetch for each wind direction bin was then measured using Google Earth Pro. Wind directions for deployments 3 and 6 were then assigned their corresponding fetch. The critical wave period (T_c), equation 2, which relied on the hourly bin-averaged pressure data (d) is based on the assumption of Deep Water Waves (DWW) with the critical condition that when the wavelength is less than two times the water depth, waves start to feel the bottom. Values of U_{wc} were compared with observed wind speeds, to identify expected times of resuspension. The results from the critical and observed wind speed comparison were further analyzed against bottom maximum wave orbital velocities and resuspension events (defined by the bottom OBS sensor).

$$T_c = \left(\frac{4\pi d}{g}\right)^{\frac{1}{2}} \tag{2}$$

$$U_{wc} = \left[1.2\left\{4127\left(\frac{T_c^3}{F}\right)\right\}\right] \tag{3}$$

SHEAR STRESS

The wave-generated bed shear stress and the current-generated bed shear stress were calculated and compared with the calculated critical bed shear stress for each. Following equation 4, the current bed shear stress (τ_{bc}) was calculated, where gravity (g) is 981 cm/s^2, the

density of water (ρ_w) is 1.025 g/cm^3, the density of the sediment (ρ_s) is 2.65 g/cm^3, the D_{50} is 9.2x10^{-4} cm, the D_{84} is 3.12 x10^{-3} cm, and the kinematic viscosity (ν) is 1.05 cm^2/sec x10^{-2}. The drag coefficient (C_d) is assumed to be 2.2x10^{-3}, based on an approximate value for a mud bed (Soulsby, 1983). The U_c term is the average current speed profile in m/s.

$$\tau_{bc} = C_d \rho_w U_c^2 \tag{4}$$

The wave shear stress on the bed was calculated using equation 4, where U_{bw} is the maximum bottom wave orbital velocity in m/s, the wave friction factor (f_w) was calculated using equation 6, where roughness (k_s) is assumed to be D_{84}. Wave amplitude (a_b) was calculated using equation 7, using the peak significant wave period (T).

$$\tau_{bw} = 0.5 f_w \rho_w U_{bw}^2 \tag{5}$$

$$f_w = e^{5.213(\frac{k_s}{a_b})^{0.194} - 5.977} \tag{6}$$

$$a_b = \frac{U_{bw}}{2\pi/T} \tag{7}$$

The total bottom shear stress is a non-linear combination of wave shear stress and current shear stress, and was calculated using equation 8 (Soulsby, 1997).

$$4\tau_{total} = \tau_{bw} + \tau_{bc}\left[1 + 1.2(\frac{\tau_{bw}}{\tau_{bc}+\tau_{bw}})^{3.2}\right] \tag{8}$$

The critical wave orbital velocity (U_m), associated with the onset of resuspension was calculated using equation 9, where T_{sig} is the peak significant wave period, H_{sig} is the peak significant wave height, d is water depth, and L is wavelength. The critical wave orbital velocity was analyzed with the observed orbital velocities to determine when the onset of resuspension occurred. The periods of expected resuspension were then compared to observed resuspension events.

$$U_m = \frac{\pi H_{sig}}{T_{sig} \sinh\left(\frac{2\pi d}{L}\right)} \tag{9}$$

CHAPTER 3

RESULTS

SEDIMENT ANALYSIS

The Lafayette River has a median grain size ranging from ~9 to 18 μm (~5-6 phi) (Fig. 5). The spatial variation of grain size within the estuary is fairly small, however, grains tend to be slightly coarser near the mouth, as observed in samples collected east of Hampton Blvd. bridge (Fig. 5).

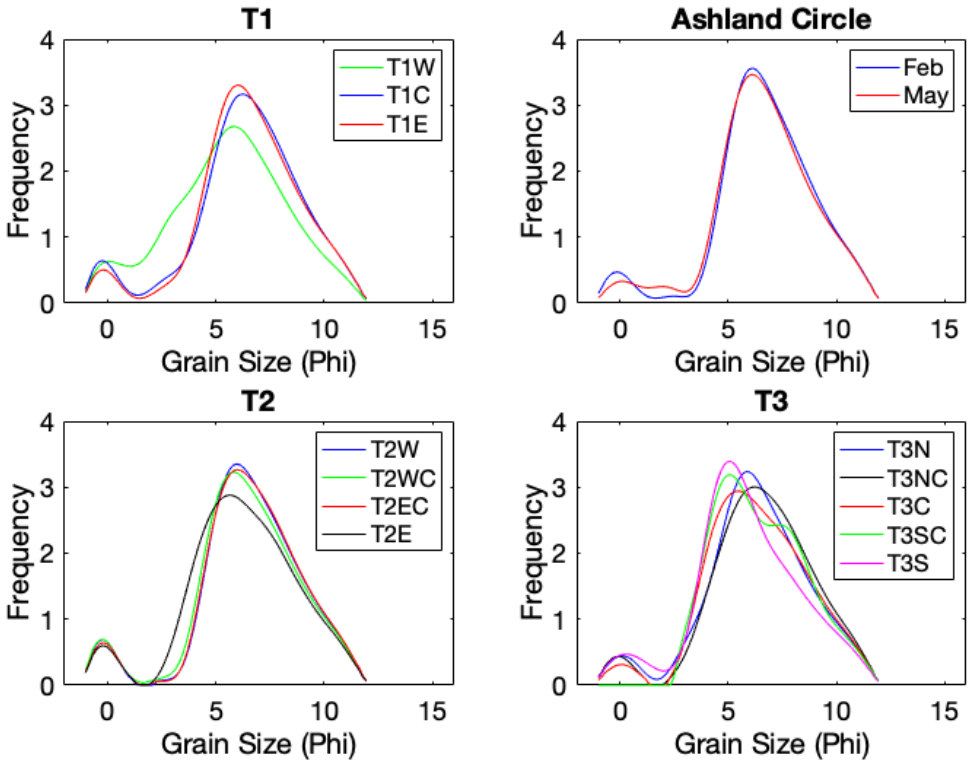

Figure 5. Grain size frequency from transect subsamples collected during deployment 4 in addition to samples collected near Ashland Circle during deployments 1 and 3. The grain size units are in phi, where larger phi values equate to smaller particles.

WAVES AND CURRENTS

In general, wave parameters that were estimated from CTD data, showed increasing wave orbital velocities during episodes of elevated wave period and wave height (Fig. 6). The maximum wave orbital velocity recorded was 9.37 cm/sec during deployment 3 and 5.20 cm/sec during the final deployment. The bottom wave orbital velocities recorded during the 3 and 6 deployments were consistently weaker than the near bed current speeds (Table 2, Figs. 7, 8).

Overall, wave orbital velocities appeared to increase when southerly or southwesterly winds were at speeds of ~5 m/s or greater (Fig. 7, 8, 9). Prolonged southerly and southwesterly winds led to increased wave orbital velocities, reduced water depth, decreased current speeds, and elevated SSC (Fig. 9). The strongest winds were observed at the beginning of deployment 6, on September 14, in association with the remnants of Hurricane Florence. Despite the strongest winds occurring during this period, the maximum wave orbital velocities were of similar magnitude to those observed during periods of weaker winds observed during deployment 3. The period of strong winds that occurred during deployment 6 were northeasterly/easterly, a scenario of reduced fetch at AC, while the relatively weaker southerly/southwesterly winds that occurred during deployment 3, are associated with a longer fetch at AC.

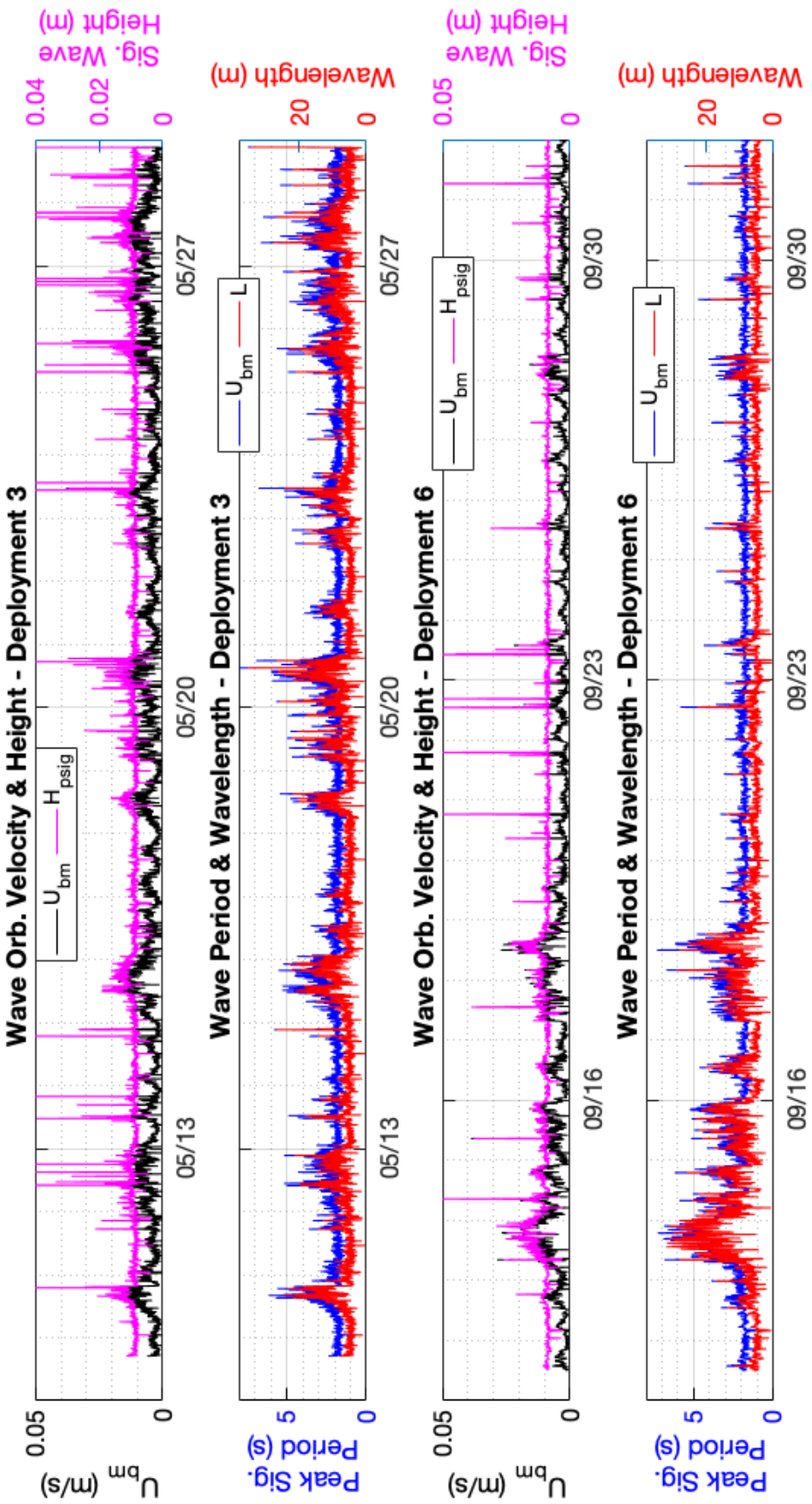

Figure 6. The first (top) panel shows maximum bottom orbital velocities and significant wave heights for deployment 3, the second panel shows peak significant wave periods and wavelengths for deployment 3. The third panel contains maximum wave orbital velocities and significant wave heights recorded during deployment 6, and the bottom panel contains peak wave periods and wavelengths observed during deployment 6.

	1	2	3	4	5	6
Mean Current Speed (Avg. of Bins 2:51)	**5.56 cm/s**	**5.76 cm/s**	**5.9 cm/s**	**5.71 cm/s**	**5.68 cm/s**	**6.0 cm/s**
Mean Bottom Current speed (Bin 2:11)	**8.15 cm/s**	**6.83 cm/s**	**7.08 cm/s**	**7.18 cm/s**	**7.01 cm/s**	**6.45 cm/s**
Max Current Speed (Avg. of Bins 2:51)	**20.79 cm/s**	**18.28 cm/s**	**20.08 cm/s**	**20.82 cm/s**	**15.81 cm/s**	**19.58 cm/s**
Max Bottom Current speed (Bin 2:11)	**22.06 cm/s**	**18.66 cm/s**	**20.72 cm/s**	**23.92 cm/s**	**18.07 cm/s**	**18.06 cm/s**
Min Current Speed (Avg. of Bins 2:51)	**0.72 cm/s**	**0.6 cm/s**	**1.0 cm/s**	**0.7 cm/s**	**0.79 cm/s**	**0.7 cm/s**
Min Bottom Current speed (Bin 2:11)	**0.46 cm/s**	**0.30 cm/s**	**0.39 cm/s**	**0.28 cm/s**	**0.39 cm/s**	**0.23 cm/s**
Mean Wave Orbital Velocity (near bed)			**0.56 cm/s**			**0.4 cm/s**
Max Wave Orbital Velocity (near bed)			**9.37 cm/s**			**5.20 cm/s**
Mean Wave period			**2.14 s**			**2.14 s**
Max Wave period			**7.95 s**			**7.31 s**
Mean Wave Height			**0.98 cm**			**0.96 cm**
Max Wave Height			**39.95 cm**			**6.88 cm**
Mean Wavelength			**6.59 m**			**6.74 m**
Max Wavelength			**35.91 m**			**31.91 m**
Mean Wind Speed	**4.56 m/s**	**4.84 m/s**	**3.76 m/s**	**3.79 m/s**	**3.11 m/s**	**5.75 m/s**
Mean near bed SSC	**32.34 mg/L**	**233.47 mg/L**	**167.98 mg/L**	**404.80 mg/L**	**216.87 mg/L**	**216.99 mg/L**
Mean Water Depth	**1.44 m**	**2.11 m**	**2.25 m**	**2.32 m**	**2.34 m**	**2.53 m**

Table 2. A summary of the average current speeds, wave orbital velocities, wind speeds, and SSC for each deployment. Wave parameters were obtained during each deployment.

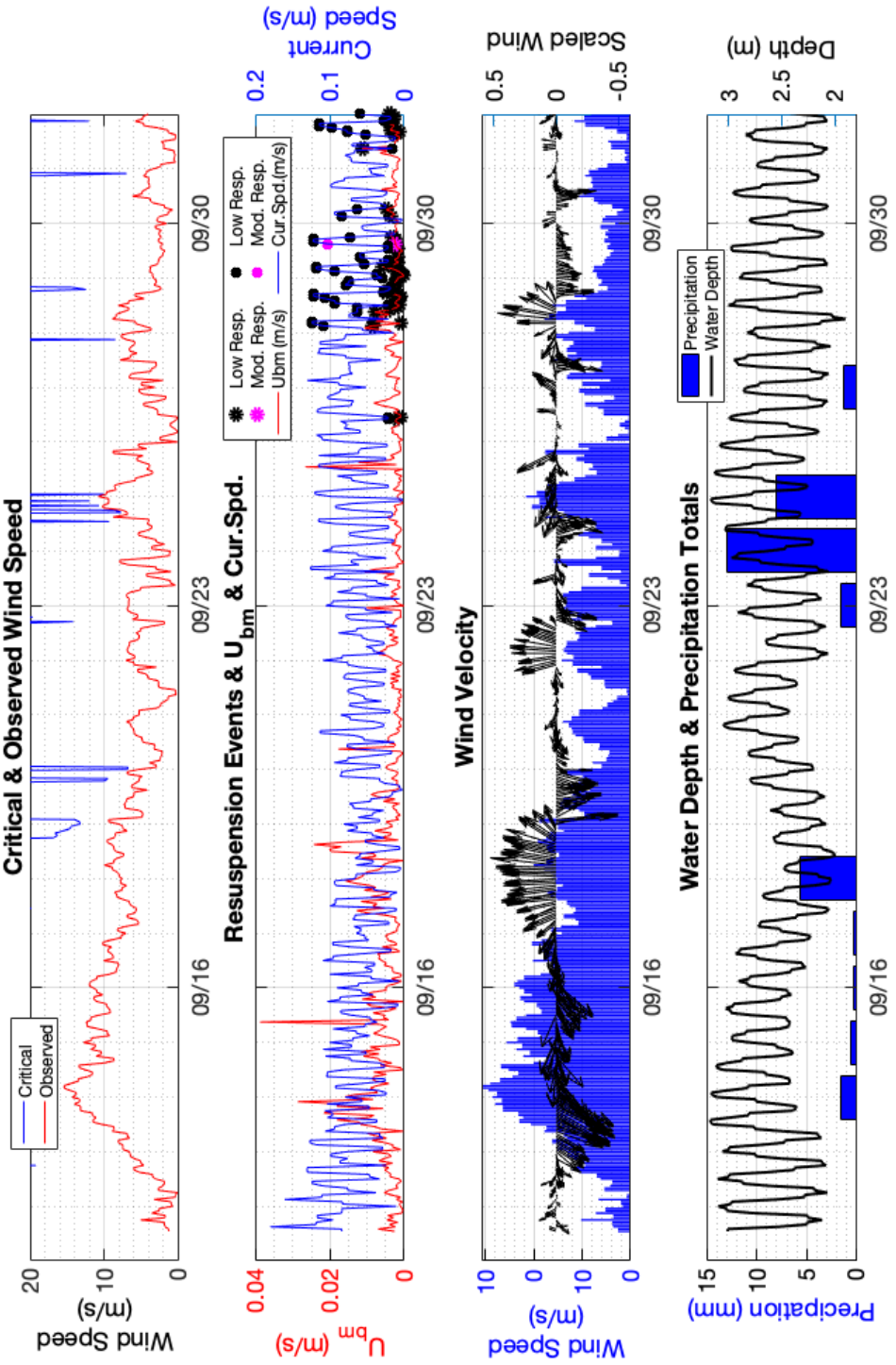

Figure 7. The top panel shows the critical wind speed required for the onset of resuspension (blue) which extends off the graph, with the observed wind speeds (red). The second panel shows wave orbital velocities (red) and current speed (blue) where resuspension events are denoted by black, magenta, and cyan dots. Current speeds strongly fluctuate as a result of the semidiurnal tides that result in 2 ebbs and 2 floods per day. Occasionally, current speeds are impacted by strong, prolonged winds. The third panel shows scaled wind vectors and observed wind speed. The bottom panel shows water depth and daily precipitation totals, during deployment 3.

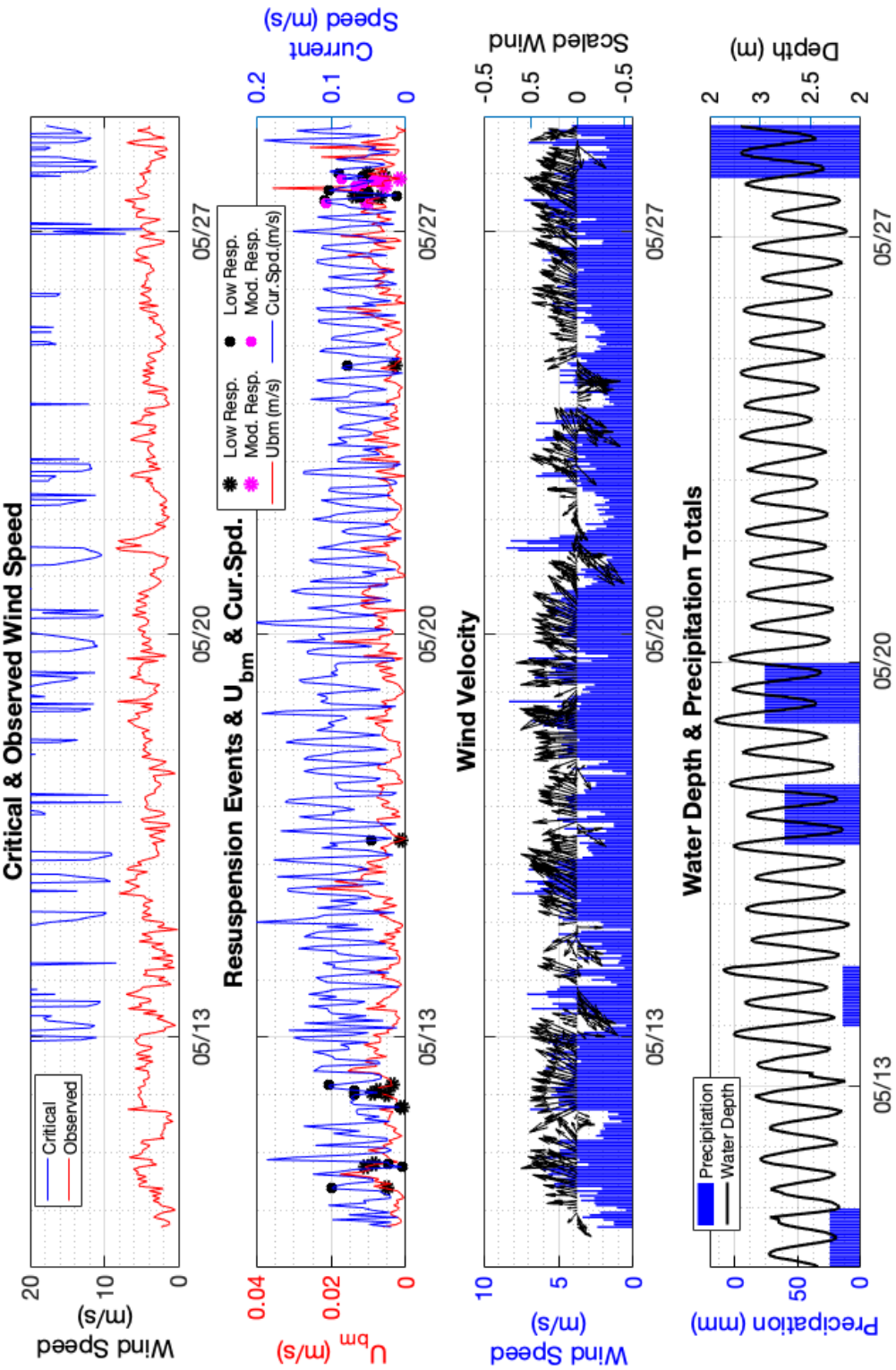

Figure 8. The first panel shows the critical wind speed required for the onset of resuspension (blue) which extends off the graph, with the observed wind speeds (red). The second panel show wave orbital velocities (red) and current speed (blue) where resuspension events are denoted by black, magenta, and cyan dots. Current speeds strongly fluctuate as a result of the semidiurnal tides that result in 2 ebbs and 2 floods per day. The third panel show the scaled wind vectors and observed wind speed, and the bottom panel shows water level and daily total precipitation, during deployment 6.

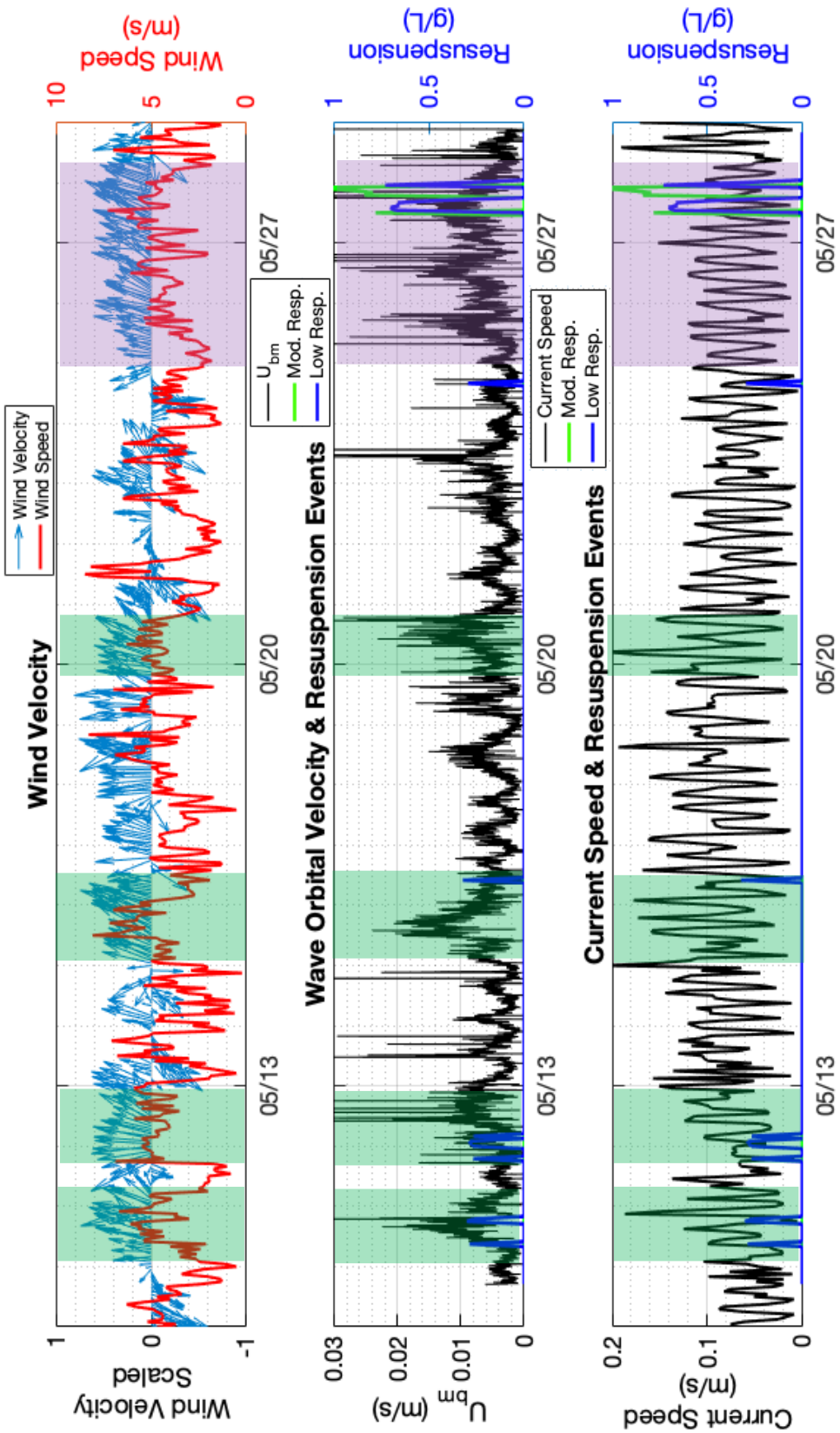

Figure 9. The green shaded regions show periods of elevated wave orbital velocities that seemingly resulted from elevated wind southwesterly winds. The purple region is an example of prolonged southwesterly winds which resulted in elevated wave orbital velocity and resuspension.

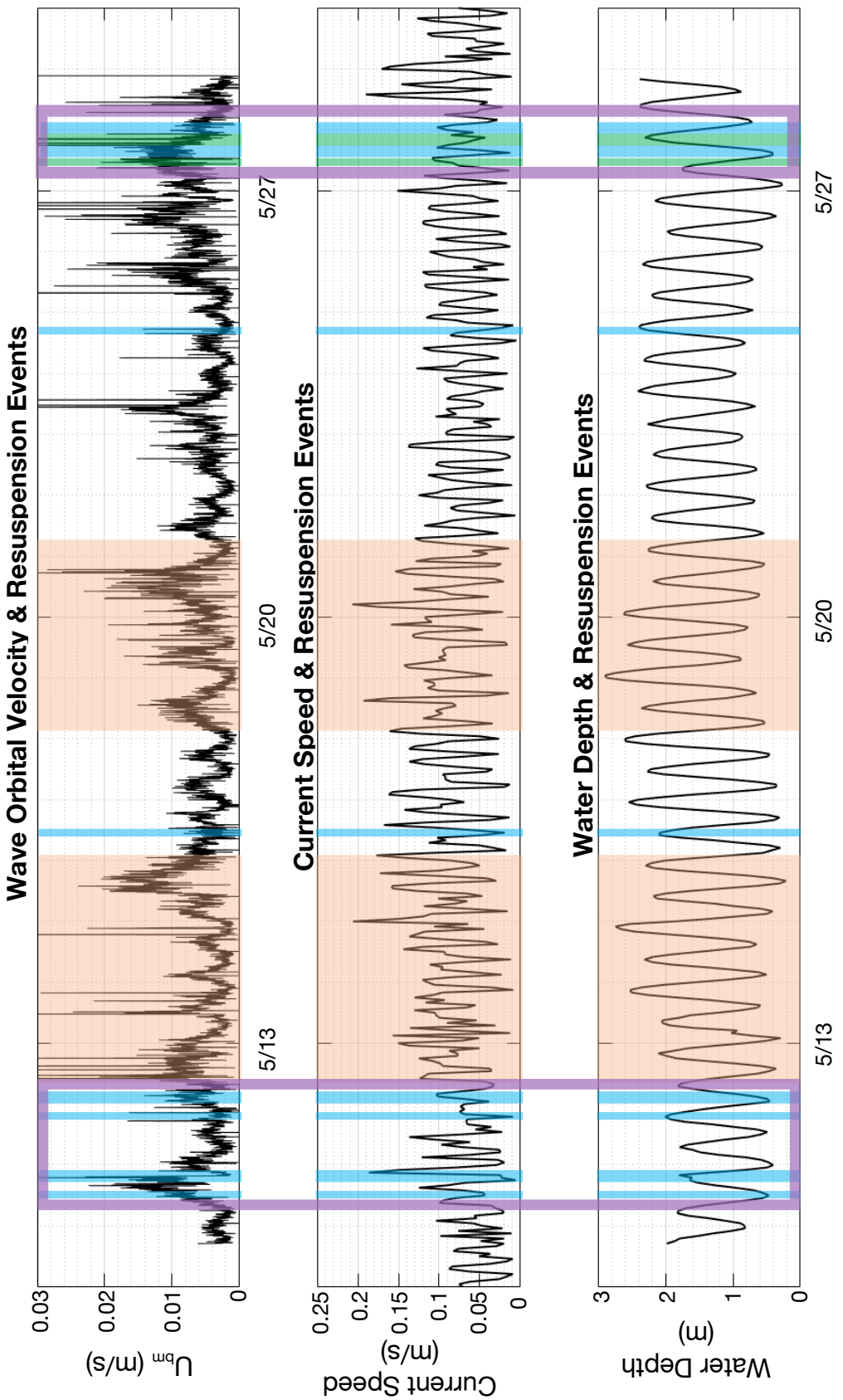

Figure 10: The purple boxes show periods where wave induced resuspension occurred, while water depth and current speeds were low to moderate. The Orange regions indicate periods of elevated wave orbital velocities coinciding with elevated current speeds and water depth, which did not result in resuspension.

The SSC and backscatter intensity recorded by the OBS and ADCP were also lower for all but the final week of deployment 6, when compared with deployment 3 (Figs. 7 and 8). Resuspension events during deployment 6 only occurred during the final week, despite the largest waves of the deployment occurring during the first week (Fig. 8). The few resuspension events that occurred during this periods seemed to result from a mix of current and wave activity (Fig.10). During deployment 3, resuspension events were more frequent and appeared to be predominantly caused by waves (Fig. 10). However, periods of increased wave orbital velocities, that often led to resuspension, seemed to have a reduced or no effect at all on resuspension when current speeds and/or water depth were elevated. The observed wave-induced resuspension primarily occurred during periods of moderate to low water depth and current speeds, suggesting that waves are causing resuspension, but the resultant resuspension is controlled by water depth and current speed. This apparent control on wave-driven resuspension appeared to occur during deployment 6 as well. When Hurricane Florence was approaching and made landfall, the strong northeasterly winds, storm surge, and spring tide that occurred on September 9, caused the water depth and current speeds to increase substantially, however as neap tide approached on September 16, current speeds began to decrease and remained relatively low despite the strong prolonged winds, while maximum near bed wave orbital velocities began to increase (Fig. 8). Prior to Florence, current speeds were substantially higher than normal, likely from the new moon on September 9, and the elevated water depth. During this period of time, wave orbital velocities were reduced, and no resuspension was recorded (Fig. 8). As wave orbital velocities increased and current speeds decreased, still no resuspension resulted, likely because of the still substantially elevated water depth (Fig. 8).

Water depth and current speeds tend to change together due to their strong tidal influence. However, wind-driven currents occasionally influenced depth and/or currents as well. On September 17,18, and 23 the winds changed and were southwesterly, which led to decreased water depths, that later rebounded as the winds died down and changed direction again. The current speeds associated with these events were typically low but on occasion could become elevated, such as on May 20, and were consequentially associated with resuspension (Fig. 7). Despite this, wind-driven currents were no more affective at causing resuspension than episodes of strong tidal currents.

REGRESSION ANALYSIS

Regression analysis of SSC from the OBS and near bed current speed, for each deployment showed weak relationships between acoustic backscatter and current speeds for deployments 1,3,4,5 and 6 (p-value <0.05; Appendices A and B). Wave orbital velocities also exhibited a weak relationship to acoustic backscatter for deployment 6, optical for deployment 3 and windspeed for both deployments (p-value < 0.05; Appendices A and B). Visual analysis of current speed does not find any specific threshold under which currents result in resuspension, but resuspension does appear to occur during or shortly after periods of winds to the northeast, when wave orbital velocities current speeds were elevated (Figs. 7 and 8). Results from a multiple regression analysis that examined the effects of near bed maximum wave orbital velocities and near bed current speeds, on resuspension visually showed a stronger, positive relationship between SSC and near bed wave orbital velocities, where currents speeds displayed little to none relation to SSC (Fig. 11).

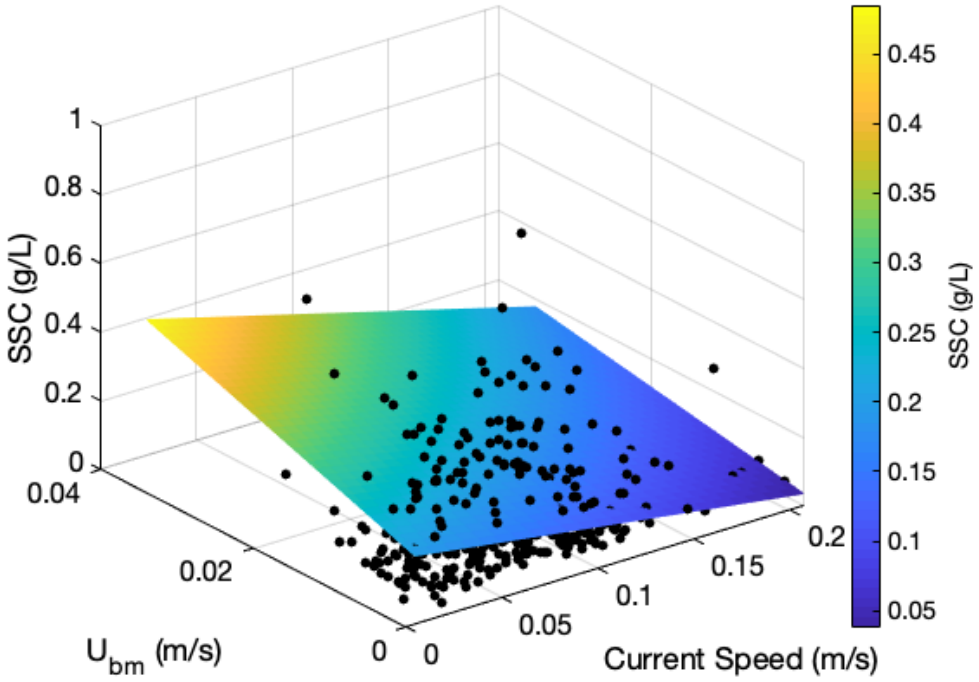

Figure 11: A multiple regression analysis of maximum near bed wave orbital velocity and average near bed current speeds with suspended sediment concentrations, where observed concentrations are represented by the black circles, while the plane is a best fir through these data. Wave orbital velocity appears to have a stronger, more positive relationship with SSC than current speed.

CRITICAL WAVE ORBITAL VELOCITY

The calculated threshold for motion due to wave orbital velocity was found to be ~0.8 cm/s, which was exceeded numerous times throughout deployments 3 and 6. These occurrences did not always correspond to resuspension events, but this threshold is only an estimate for the initiation of resuspension; the magnitude of may not meet the event criteria as defined by this study. Southwesterly winds at speeds of >5 m/s typically generated wave orbital velocities >1 cm/s, with waves >2-3 cm/s and capable of resuspending or significantly aiding in the resuspension of sediment (Figs. 7, 8, 9). However, there were a few cases were wave orbital

velocities exceeded 1 cm/s during deployment 6, with northeasterly and easterly winds at speeds ≥ 10 m/s. Resuspension events were also not exclusive to periods of wave orbital velocities ≥ 2 cm/s (Fig. 10); current speed also seems to have a role in resuspension. During deployment 6, there are a few cases where wave orbital velocities were elevated but current speeds were relatively low, and there was no resuspension, while at other times strong current speeds accompanied by wave orbital velocities < 1 cm/s were observed and there was resuspension (Fig. 8).

CRITICAL WIND SPEED

To further investigate the effect wind had on wave-driven resuspension, the critical wind velocities were compared with the observed wind velocities. During deployment 3, the critical wind velocity threshold was never met, although there were numerous instances when it was close. Typically, wave orbital velocities exceeded 1 cm/s when the critical wind speed was within 5 m/s of the observed speed for prolonged periods during or a few hours prior to the elevated wave orbital velocity. Times when observed and critical wind speeds were less than 5 m/s from one another did not correlate well with the observed resuspension events, as shown in figure 9.

SHEAR STRESS

The wave-generated bed shear stress calculated for deployment 3 was, on average, lower than current shear stress (0.0019 dynes/cm^2 and 0.1479 dynes/cm^2, respectively). Deployment 6 had opposite results where the average wave shear stress (0.3433 dynes/cm^2) was larger than current shear stress (0.1068 dynes/cm^2). The critical shear stress was approximated as between

0.4 to 0.9 dynes/cm^2 based on results from a study with similar bed composition (Bale et al., 2006). The total wave-current shear stress and the current shear stress exceeded this threshold many times throughout deployment 3 and on a few occasions during deployment 6, although resuspension events did not appear to occur as a result.

NUTRIENT ANALYSIS

In general, combined nitrate & nitrite as well as ammonium concentrations at a nearby water quality monitoring station increased with depth, with highest concentrations occurring in the bottom waters (Figs. 12, 13). Phosphate samples, however, did not exhibit a patter that varied with depth (Fig. 12).

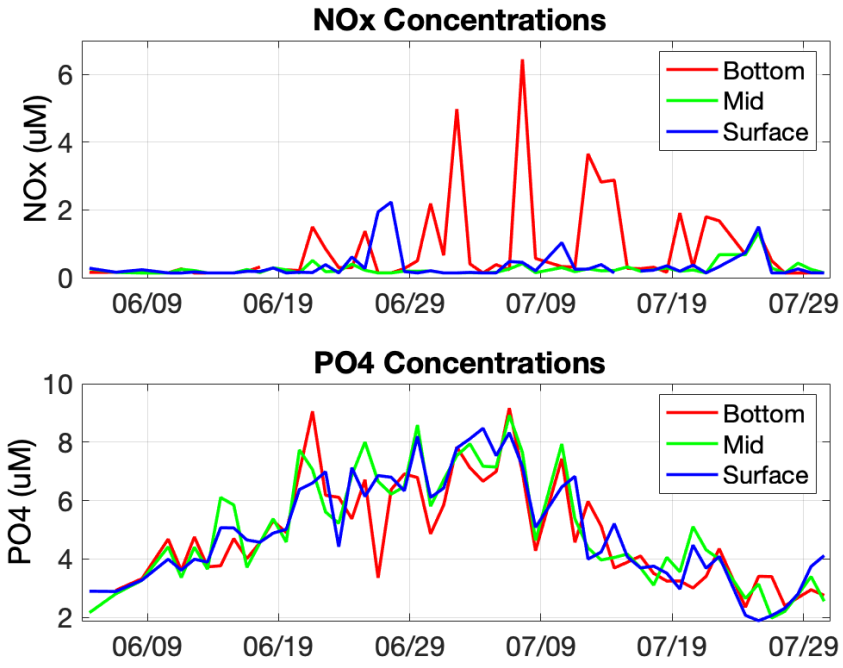

Figure 12. Top panel: Combined NO_3^- NO_2^- measured in µM at various depths, bottom concentrations were commonly higher than other depths of the water column. Bottom panel: PO_4^{3-} measured in µM at various depths of the water column, surface concentrations tend to be higher than other depths.

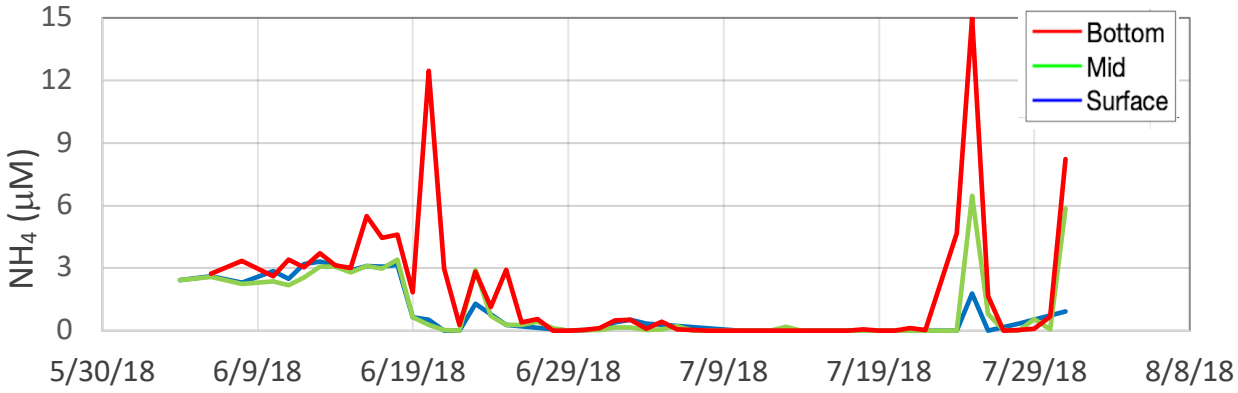

Figure 13. NH_4^+ measured in µM at various depths shows bottom concentrations were commonly higher than other depths of the water column.

DINOFLAGELLATE BLOOMS

Three different dinoflagellate species bloomed in succession of one another during the summer of 2018. A bloom of *Gymnodinium instriatum* was observed on June 1 2018, that was succeeded by a bloom of *Akashiwo sanguinea* on July 3 2018, and a bloom of *Margalefidinium polykrikoides* beginning on August 7 2018.

RESUSPENSIONS LINK TO HIGH CHLOROPHYLL

From May 7 through October 1, more than 60 resuspension events were observed where resuspension events were defined by near bed SSC reaching or exceeding 0.5 g/L (App. C and D). Events were divided into three different categories based on SSC; events that were classified as “low” had SSC’s greater than or equal to 0.5 g/L but less than 1.5 g/L, “moderate” events were SSC’s greater than or equal to 1.5 g/L but less than 3 g/L, and “high” events were SSC’s greater than or equal to 3 g/L. Many of these events coincided with or were followed by

increases in bottom nutrients concentrations which often times were subsequently followed by elevated Chl *a* as well (Figs. 14-17).

Resuspension events were infrequent during the *G. instriatum* bloom that occurred at the beginning of June, but these events began to increase in magnitude on June 10 when about 1 g/L of sediment was resuspended followed by an increase of both NH_4^+ and $NO_3^- + NO_2^-$ concentrations on the June 11 (Fig. 14). Smaller, but frequent resuspension events were observed from June 11 onward, and were followed by even higher bottom water concentrations of NH_4^+ and $NO_3^- + NO_2^-$ (Fig. 14). Chl *a* concentrations increased substantially from June 12-14. From June 12-14th, winds strengthened and were southwesterly, at the same time, current speed strengthened, and consequently so did resuspension (Fig. 14). Resuspension events during this period resulted in bottom SSC's of ≥1 g/L, which again were followed by small increases in NH_4^+ concentrations in bottom waters on June 13-14. Concentrations of $NO_3^- + NO_2^-$ dropped below detection limits at this point, while Chl *a* remained elevated. On June 15th Chl *a* concentration began to decrease, but another resuspension event of ~ 1 g/L, late on the 15th led to increased NH_4^+ and $NO_3^- + NO_2^-$ on the 16, and Chl *a* on the 17th (Fig. 14).

The largest resuspension event during summer 2018 occurred on June 20 when SSC reached almost 6 g/L. This event was followed by a near immediate increase of NH_4^+, $NO_3^- + NO_2^-$, and PO_4^{3-} concentrations, and then increased Chl *a* concentrations which persisted until the June 23 (Fig. 15). On the June 27-28 smaller resuspension events occur and were followed by smaller increases of all nutrients except NH_4^+ drops below detection limits on the 28 (Fig. 15). These events are again followed by a spike in Chl *a* concentrations on June 29-30 (Fig. 15), which was followed by a transition of dominate species.

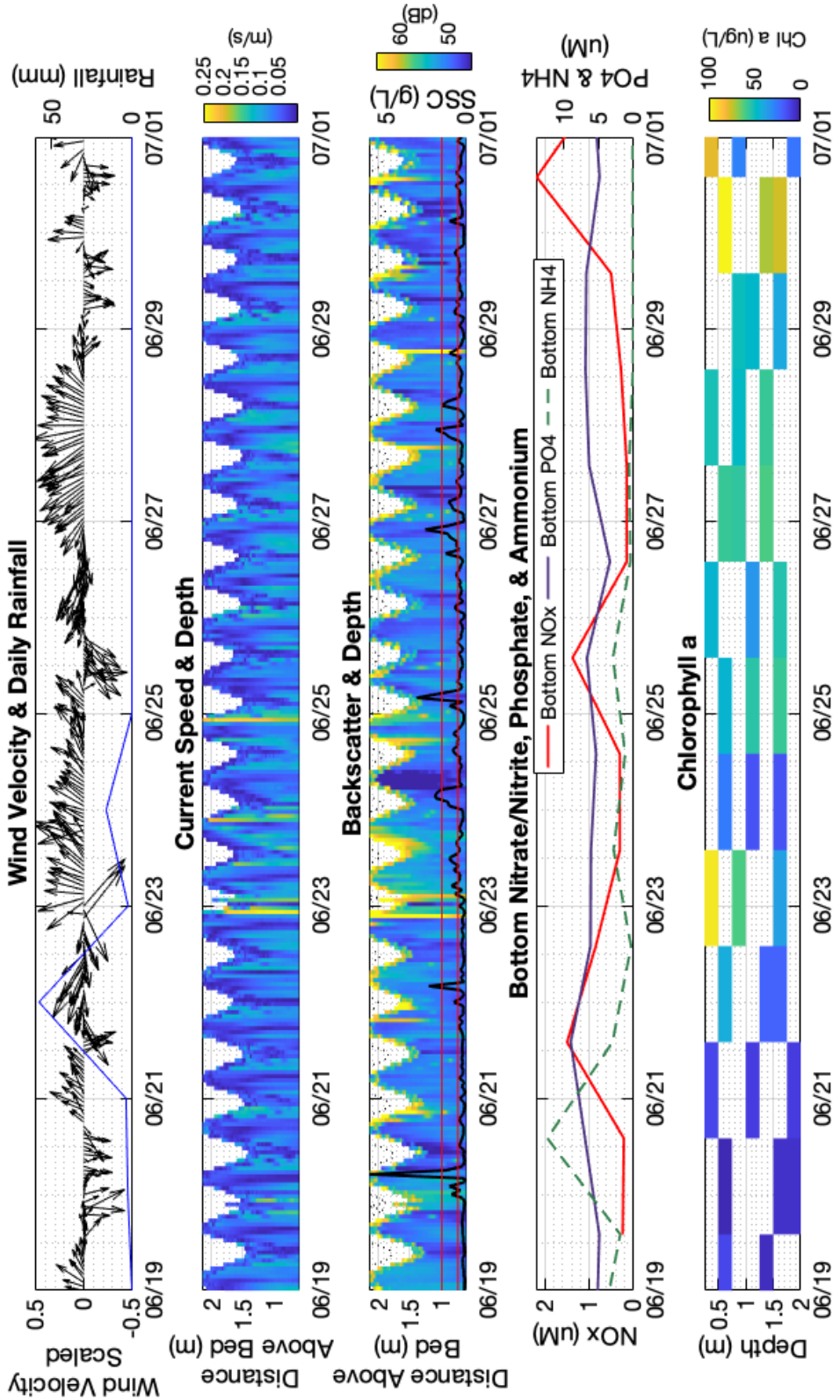

Figure 14. Top panel: Scaled wind velocity and rainfall total. Second panel: Current speed. Third panel: Acoustic backscatter and near bed SSC (g/L) recorded by the bottom OBS, showing resuspension events. The red lines represent the 0.5 g/L and 1.5 g/L resuspension thresholds. Fourth panel: Bottom nutrient concentrations. Bottom panel: Chlorophyll a concentrations from multi depth water sample analysis.

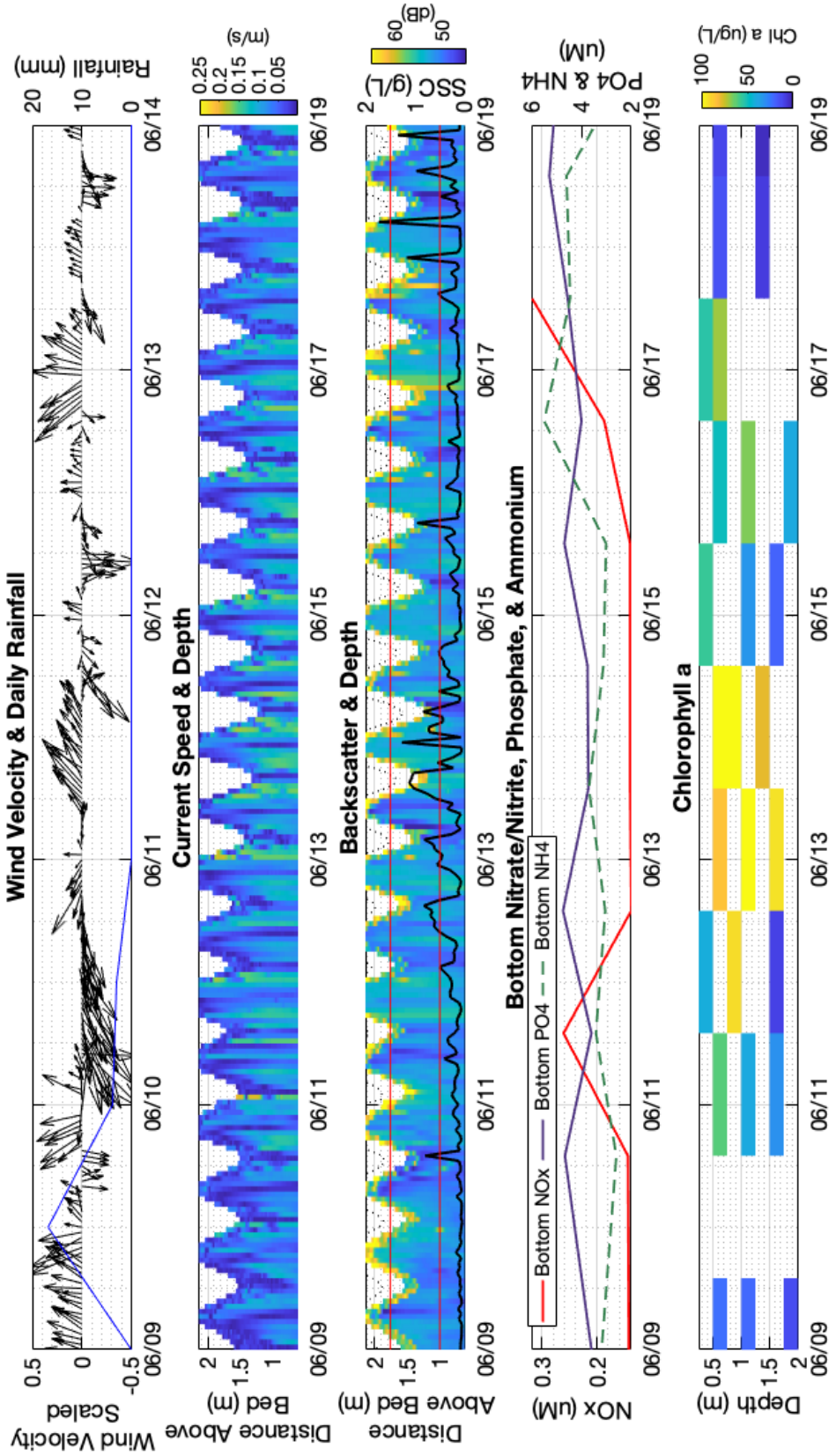

Figure 15. Top panel: Scaled wind velocity and rainfall total. Second panel: Current speed. Third panel: Acoustic backscatter and near bed SSC (g/L) recorded by the bottom OBS, showing resuspension events. The red lines represent the 0.5 g/L, 1.5 g/L, and 3.0 g/L resuspension thresholds. Fourth panel: Bottom nutrient concentrations. Bottom panel: Chlorophyll a concentrations from multi depth water sample analysis. The largest resuspension event occurred on 6/20.

A series of low resuspension events occurred on 1 and 2 of July which were followed by increases in all nutrients measured on the 2, then Chl *a* on the 3 and 4 commencing the *A. sanguinea* bloom. From July 3 through 5 there are several low and a few high events that result in minimal nutrient increases, all while Chl *a* remained elevated (Fig. 16). The second-strongest resuspension event occurred on July 6, which lead to a significant increase in NO_3^- +NO_2^- and increased Chl *a* throughout the water column as on July 7 (Fig. 16).

As July progressed, Chl *a* remained elevated, while consistent low or just below low, events dominated, while NH_4^+ was near detection limits, and NO_3^- +NO_2^- increase significantly shortly after an elevated current speeds and acoustic backscatter on July 12 (Fig. 16). After July 20, storms caused significant rainfall with strong southeasterly winds that resulted in only a few low resuspension events. Despite minimal resuspension, nutrient concentrations increased on the 21 and 25, likely from runoff due to the storms. Chl *a* increased as the conditions ease on the 25, through the end of July (App. E, F, and G).

For the resuspension events that resulted in increased nutrients and/or Chl *a,* a typical sequence is as follows: sediment was resuspended, nutrient concentrations increased within 1-2 days, and Chl *a* concentrations increased after 2-3 days. The lag time between a mixing event and the observance of increased Chl *a* is in agreement with results from Morse et al. (2014).

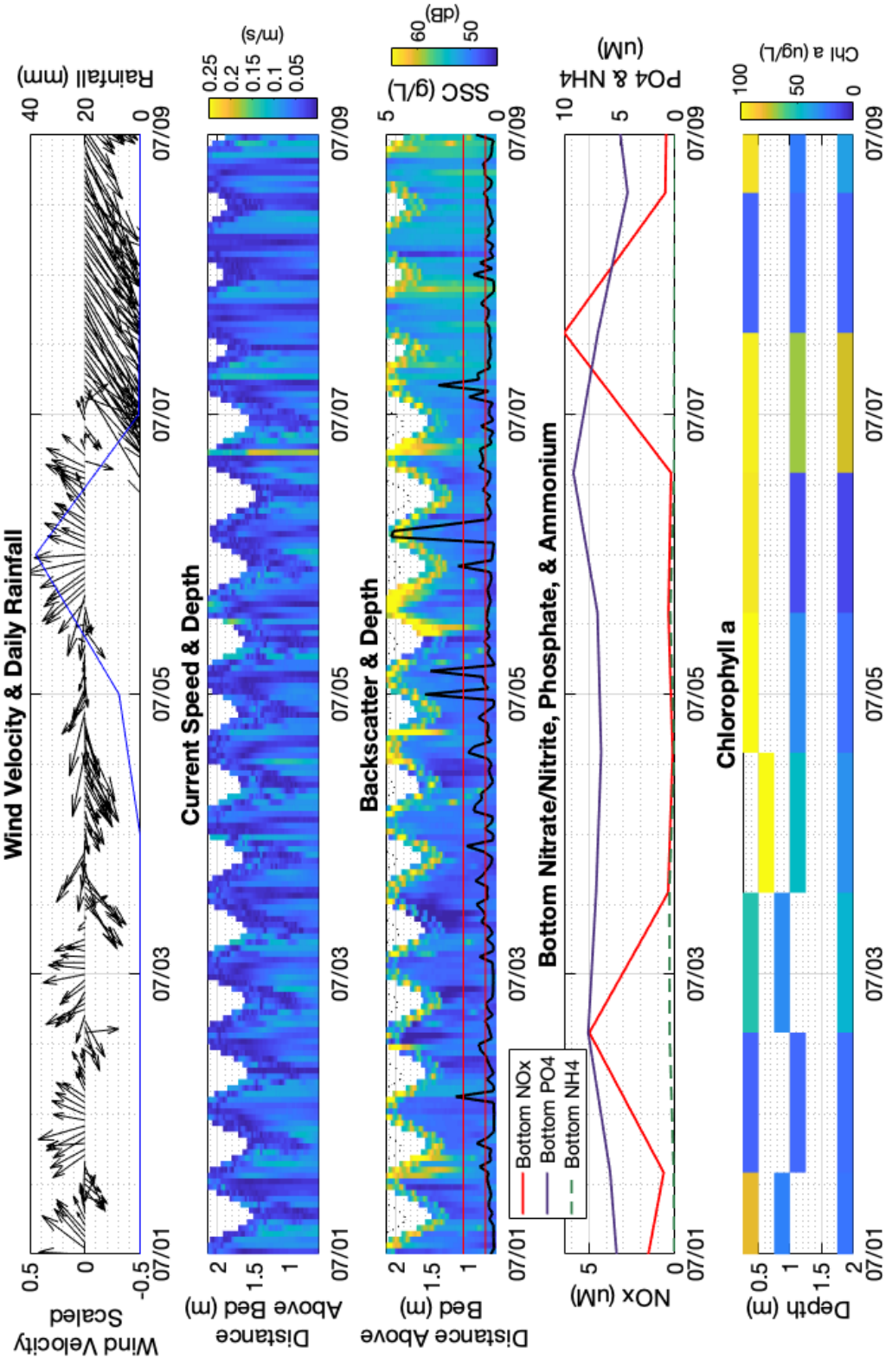

Figure 16. Top panel: Scaled wind velocity and rainfall total. Second panel: Current speed. Third panel: Acoustic backscatter and near bed SSC (g/L) recorded by the bottom OBS, showing resuspension events. The red lines represent the 0.5 g/L, 1.5 g/L, and 3.0 g/L resuspension thresholds. Fourth panel: Bottom nutrient concentrations. Bottom panel: chlorophyll a concentrations from multi depth water sample analysis.

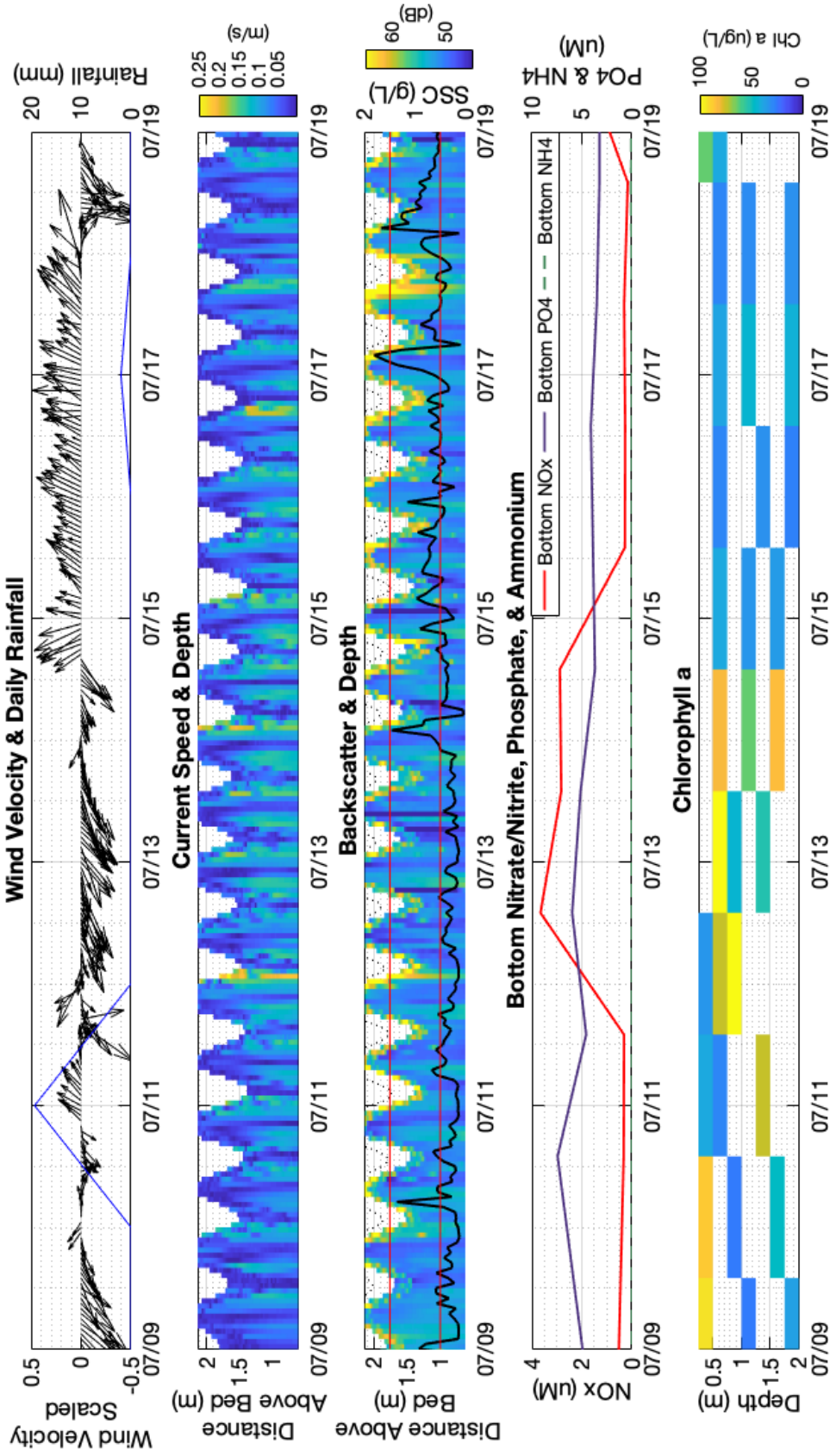

Figure 17. Top panel: Scaled wind velocity and rainfall total. Second panel: Current speed. Third panel: Acoustic backscatter and near bed SSC (g/L) recorded by the bottom OBS, showing resuspension events. The red lines represent the 0.5 g/L and 1.5 g/L resuspension thresholds. Fourth panel: Bottom nutrient concentrations. Bottom panel: Chlorophyll a concentrations from multi depth water sample analysis.

CHAPTER 4

DISCUSSION

RESUSPENSIONS LINK TO HIGH CHLOROPHYLL

Numerous resuspension events followed by increased nutrient concentrations and Chl *a* concentrations were overserved from the start of June throughout July in the Lafayette River. The lag times between sediment resuspension, bottom water nutrient enrichment and elevated Chl *a* concentrations were consistent with the 2-7 day lag times between storms and blooms observed previously (Morse et al., 2014).

The link between sediment resuspension and elevated nutrient concentrations was supported by observations of increased ammonium and nitrate+nitrite in bottom water as compared to mid-water or surface concentrations. Phosphate did not follow patterns similar to N concentrations which is expected since the Lafayette River is not P limited, rather its N limited. Although, nutrient enrichment might be expected during/after significant rainfall events, due to loading from surface-water runoff (Paerl et al., 2001; Howarth et al., 2006; Dwight et al., 2011), runoff into the Lafayette River likely results in a buoyant lens of freshwater at the surface, due to mesohaline properties of the estuary. Additionally, estuarine sediments have been recognized as a source of nutrients, where a benthic-pelagic coupling delivers organic matter that was produced in the water column, to the benthos where organic matter can be stored, decomposed, and regenerated into nutrients (Kemp and Boynton, 1996; Jahnke et al., 2003; Corbett, 2010). The commonality of seasonal blooms which occur in Lafayette River, (Morse et al., 2014; Egerton et al., 2014), likely supply its benthos with organic matter initiating the benthic-pelagic coupling. The flux of nutrients associated with advection or sediment resuspension are significantly higher than fluxes associated with the diffusive flux of nutrients from stable (passive) sediments

(Fanning et al., 1982; Simon, 1988; Kristensen et al., 1992; Sondergaard et al., 1992; de Jonge et al., 1995; Corbett, 2010). Thus, resuspension events observed in the Lafayette River are likely a significant source of fuel for algal growth, especially during periods of drought, when there's not supply via runoff. Sediment resuspension observed appeared to advect nutrients into the water, typically leading to greater concentrations in bottom water. This supply of nutrients bottom water appeared to support and/or stimulate Chl *a* abundance that was dominated by dinoflagellates throughout this study and may have given advantage to these organisms over other phytoplankton, due to their motility within the water column.

Sediment resuspension in the upstream region of the Lafayette River is more likely to contain and consequentially resuspend cysts because dinoflagellate cysts are found in higher concentrations among muddy sediments, decreasing in concentration with increasing grain size (Brown et al., 2012). While the spatial variability of grain size within the Lafayette River is fairly small, there is a slight fining of sediment upstream, where the AC station is located. Prior studies have observed the Lafayette River acting as a seedbed for *M. polykrikoides* blooms, in addition to the aggregating and blanketing the bed as a bloom diminished (Morse et al., 2011).

The resuspension of sediment within this highly productive system may be essential for the germination of the cysts to occur. The oxic zone of estuarine sediments, where germination can occur, is typically 5 mm or less, and is often absent below 1 mm (Fenchel, 1992). Sediment resuspension can either reoxygenate sediments or move cysts to an aerobic sediment layer, where germination is possible. Additionally, resuspension can advect cysts from low-light condition to more optimal light conditions which have been shown to increase the frequency of germination (Anderson et al., 1987; Kremp and Anderson, 2000; Kremp, 2001). Determining controls on cyst germination were beyond the scope of this study however, results showed Chl *a* increased within

2-5 days of resuspension events, thus the advection of cysts to an aerobic zone or to a zone of greater light intensity, allowing germination to occur and/or at a higher frequency cannot be ruled out.

CAVEATS SURROUNDING RESUSPENSION EVENTS

Dinoflagellate blooms are regulated by a variety of factors, ranging from temperature, salinity, and grazing. Of the many resuspension events that were observed in summer 2018, not all led to subsequent increases in Chl *a*. There are a number of explanations as to why this is the case. For example, storms with high winds and turbulence are also primary disruptors of blooms (Lee, 2006; Morse et al., 2014; Lim et al., 2015; Filippino et al., 2017). Storms associated with large amounts of rainfall can cause "wash out" of algal populations if cells are entrained in high flow events (Filippino et al., 2017). Further, sediment resuspension can introduce turbidity into the water column that can block light penetration thus inhibiting photosynthesis.

Due to the relatively low frequency of nutrient measurements (daily) compared to resuspension measurements (hourly), if there were already dense algal populations in the water when resuspension occurred, resuspended nutrients may have already been taken up, before the daily nutrient samples were collected. Another factor that could limit the amount of primary production associated with the resuspension of sedimentary nutrient inputs is the rate of sedimentary nutrient regeneration. For example, if the frequency and magnitude of resuspension events is faster than rates of sedimentary nutrient regeneration then this would limit nutrient inputs during resuspension events. Runoff associated with rain events can also be a source of nutrients to the Lafayette River, however, the effects of runoff on nutrient concentrations near the bed were assumed to be minimal because the fresh water is buoyant; thus it is confined to

the surface where phytoplankton would likely utilize nutrients associated with these inputs. However, storms that occurred during late July brought significant rainfall, strong southeasterly winds, and minimal resuspension events, that were eventually followed by increased nutrient concentrations and then Chl *a*. Significant rainfall events can lead to stratification of the Lafayette River, shifting it from a well-mixed estuary, to a partially mixed estuary (Blair et al., 1976). Increased stratification, in addition to increased nutrient input via runoff, both of which have been observed to promote algal growth locally (Morse et al., 2013).

Acoustic backscatter and SSC from the OBS did not exhibit a strong correlation, which is not a tremendous surprise (App. H). Measurements of backscatter using the ADCP ranged from ~60 cmab up to the water's surface while the OBS recorded at ~50 cmab and ~3 cmab Since the sensors were measuring different portions of the water column, the acoustic sensor may have missed events that the OBS would have captured, as the wave boundary layer is typically <5 cm; well below the lowest bin of acoustic measurements. In addition to the sampling depth difference, these sensors are sensitive and dependent on different environmental phenomena and factors since one relies on the transmission of sounds while the other, relies on light. Acoustic backscatter is dependent on water temperature, salinity, and pressure but is not prone to biological fouling, while optical backscatter is highly susceptible to biological fouling (Schoellhamer, 1993; Gartner, 2004). Fouling of the optical sensor face can either reduce the amount of backscatter received by the sensor, giving a false low reading or can increase the backscatter, resulting in a false high reading (Downing, 2006). To reduce the effects of fouling both the ADCP and OBSs were treated, which reduced the amount of fouling observed but not all.

Phytoplankton have been shown to cause interference with OBS measurements of SSC when present in high concentrations, one study in particular found a suspended solids signal of ~ 100 mg/L when phytoplankton concentrations were high and suspended sediment was low (Schoellhamer, 1993). Despite documented interference OBS measurements, phytoplankton cells have a spectral backscatter coefficient that's 4-60 times lower than mineral particles, making their scattering abilities sufficiently lower than sediment (Downing, 2006; Ahn et al., 1992; Stramski and Kiefer, 1991). For the purpose of this study, the effects of interference from blooms are considered negligible since the lower limit of defined resuspension events required suspended solid concentrations of 500 mg/L or more.

CAUSE OF RESUSPENSION

It is well established that sediment resuspension is predominately caused by current or wave motion that erodes surface particles and re-entrains them into the water column (Nichols, 1992; Green and Coco, 2012). In shallow micro-tidal environments, such as the Lafayette River, the resuspension of material is typically controlled by wind (Lawson et al., 2007; Booth et al., 2000; Nichols, 1992) due to the reduced water depth, tidal currents are often weak and wind-waves can penetrate to the bed (You, 2005). In fact, wave-forced resuspension by wind, in shallow areas, has been shown to be 3-5 times more effective than tides at resuspending sediment, despite the limitations fetch imposes on waves (Brand et al., 2010; Booth et al., 2000).

Wind speed, fetch, and water depth appeared to control observed wave orbital velocities in the Lafayette River, consequentially wave orbital velocities were an order of magnitude less than current velocities. Despite this, waves were more often associated with resuspension than elevated current velocities. This may be due to difference between wave and current motion;

waves exhibit oscillatory motion, which is more effective at eroding and resuspending materials than currents, which have unidirectional motion and are more effective at transporting materials.

Considering the controls on wave generation in the Lafayette River, fetch is shortest at AC during northerly and northeasterly periods of winds, but is substantially longer during southwesterly winds. However, local seasonal wind patterns result in weak southerly and southwesterly winds and strong northerly and northeasterly winds (App. I, J, K, and L). Subsequently, weak southerly and southwesterly winds generated waves of the same magnitude as strong northerly and northeasterly winds (Fig. 17). An example of the limitations fetch had on wave orbital velocity occurred during deployment 6, when northeasterly winds reached ~15 m/s, but resulted in wave orbital velocities comparable to those generated by southwesterly winds of less than half the speed. Results overall showed southwesterly winds with speeds of ~5 m/s and greater typically generated wave orbital velocities of >1 cm/sec, and were associated with resuspension events (Figs. 8, 9), while northeasterly and easterly winds required speeds of ≥ 10 m/s to generate waves of comparable velocity, but didn't result in resuspension.

Prolonged southerly and southwesterly winds led to increased wave orbital velocities, reduced water depth and current speeds, and elevated SSC, which suggests a wave-current interaction is likely present. However, the CTD and ADCP were not able to capture wave direction, thus investigating this suspected interaction was not possible. The prolonged southwesterly winds may have generated wind-driven currents, which led to the decreased water levels that were commonly observed during these conditions and likely aided in wave-generated resuspension, since these wind-driven currents were not often not associated with increased current speeds and were thus unlikely to be the primary force behind observed resuspension.

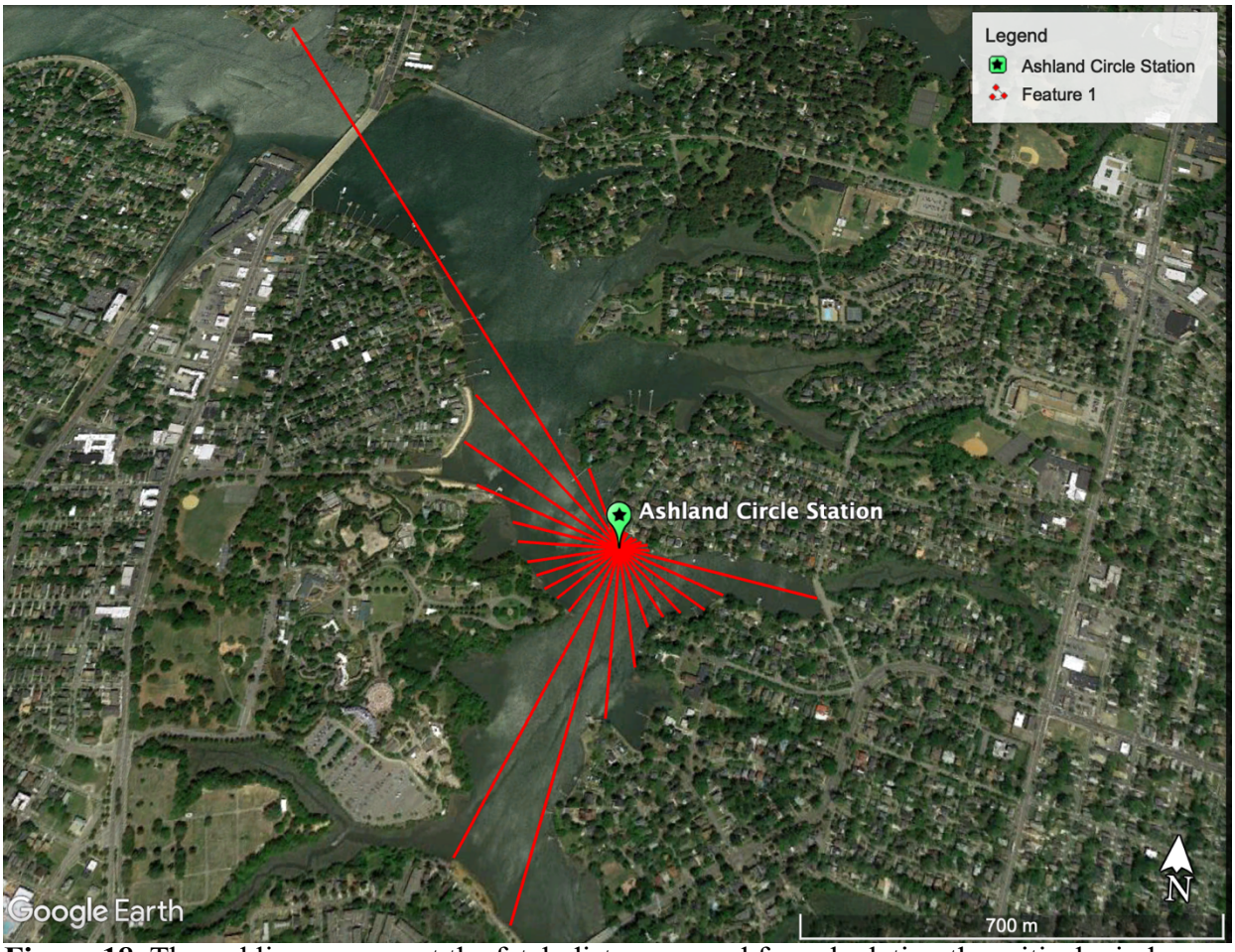

Figure 18. The red lines represent the fetch distances used for calculating the critical wind velocity. Northeasterly winds are associated with the shortest fetch at AC station.

Based on the calculated wavelength and observed water depths, waves observed during deployments 3 and 6 were Intermediate Water Waves (IWW) but on occasion met the criteria for DWW or Shallow Water Waves (SWW), according to the Shoreline Protection Manual's definition. IWW have a wave base that is greater than 0.04 but smaller than 0.2, and an elliptical orbit that reaches the bed prior to decay. However, the motion of these orbitals is not as powerful near the bed as a wave that meets the SWW criteria, thus limitations imposed by water depth are just as important as fetch. In other words, the observed wavelengths are often too short, relative to water depth, to result in sufficient force on the bed to generate significant resuspension.

Deployment 6 had more instances of DWW than deployment 3, in addition to having fewer resuspension events than deployment 3 (Figs. 8, 9), which were suspected to have resulted from the substantially elevated water depth associated with the movement and arrival of Hurricane Florence. Despite DWW not having the capability to resuspend materials, elevated SSC and backscatter intensity were observed concurrently with waves of this class. These occasional instances of elevated SSC, that were recorded during periods of DWW, likely resulted from resuspension due to elevated current speeds (tidal or wind-driven), suggesting currents alone, or with minimal aid of waves motion, can resuspend sediments at AC. However, some of the observed resuspension events may have resulted from resuspension at another location within the estuary, that was advected to the AC study site. Resuspension throughout the Lafayette River varies spatially since the estuary varies morphologically. Unfortunately, the data from this study could not fully differentiate SSC generated by resuspension from SSC associated with advection. There were a few resuspension events that were not explained by waves or currents and may have resulted from the advection of sediments already in suspension or biological interference from fish feeding on algae that grew off from other portions of the sensor's housing (Schoellhamer, 1993).

Only deployments 3 and 6 included the high-frequency (6 Hz) CTD necessary to calculate wave parameters in this shallow-water, fetch-limited system. Because deployments 4 and 5 (i.e., when blooms occurred) lacked these measurements, determining the specific cause of resuspension remains a challenge. All other deployments only included the ADCP, which sampled at a rate of 1 Hz and therefore could only detect frequencies up to 0.5 Hz. Putting this into perspective, the wind wave frequency band ranges from about 0.003 Hz beyond 10 Hz., while frequencies around 0.3 Hz are associated with the most energy within the wave band.

Therefore, the ADCP could not fully capture wave motion, while the CTD was able to cover most, but not all of the spectrum. In addition, higher-frequency waves attenuate much quicker with depth and thus are less likely to be recorded by the CTD (Gibbons et al., 1983). While the complex geometry of the study area and inherent challenge of working in fine-grained sediments are certainly confounding factors, it is likely that the poor correlation between observed wave orbital velocities, wind parameters as well as resuspension events resulted in part from sampling-frequency limitations.

Despite sampling limitations, these data showed sediment resuspension primarily occurring as a result of wave orbital velocities ≥ ~2 cm/s, coinciding with southwesterly winds ≥ 5 m/s, relatively weak to moderate current speeds and low to moderate water depths (Figs. 7, 8, 9). Periods of relatively fast current speeds and elevated water depth appeared to negate the effects of elevated wave orbital velocities on sediment resuspension. Elevated water depth likely caused the orbital motion of these short wind-driven waves to dissipate prior to reaching the estuary's bed, while the current speeds may have had a more complex effect on mitigating wave-driven resuspension that could have resulted from the direction of the current and waves. Additional critical components to resuspension events are morphology and fetch. The resuspension events observed were primarily associated with periods of southwesterly winds, which due to the shape of the estuary, had a larger fetch, and led to water levels decreasing in this lower branch of the estuary, subsequentially reducing current speeds as well. Thus, wind-driven currents are another key factor for resuspension at AC station, not because of increased current speeds, but rather, due to decreased current speeds and water depth.

CHAPTER 5

CONCLUSION

From this study, sediment resuspension at AC station appears to be largely controlled by wind-driven waves, but occasionally resulted from current activity (tidal and wind-driven). Currents are typically not the leading cause of sediment resuspension in shallow microtidal estuaries due to the episodic flow reversal and consequential reduced current speeds, whereas the shallow waters allow the short wind-driven waves that occur in estuaries, to interact with the bed. Despite the role of wind-driven waves in this system, water depth and current speeds were able to negate the effects of elevated wave orbital velocities. Depth's control on wave-driven resuspension is not unexpected as observed waves were relatively short, limiting interaction with the bed. Mitigation of wave-induced resuspension resulting from elevated current speeds appeared to occur and is likely a function of current and wave direction induced interference, however, this particular phenomenon remains unresolved due to sensor limitation. In addition to increased water depth, fetch limitations were able to moderate intense wave activity during periods of strong northeasterly winds. Despite wind-driven waves predominantly causing resuspension at AC, currents were on average, the largest source of shear stress on the bed, due their speeds often being an order of magnitude higher than waves. Future work should include higher frequency measurements of waves and currents, wave direction, as well as measurements of waves and currents at other locations within the Lafayette River. These measurements would help describe the interaction between waves and currents better, and would capture the spatially variability of currents, waves, and resuspension within the estuary.

Numerous observations of resuspension events followed by increased bottom water nutrient concentrations and/or Chl *a* concentrations suggests that resuspension of cysts and

nutrients may aid in the development of dinoflagellate blooms observed in the Lafayette River. The link between the succession of sediment resuspension and algal blooms was supported by observations of sediment resuspension followed by elevated bottom water ammonium and nitrate+nitrite concentrations and increases in Chl *a* concentrations. The time lags associated with sediment resuspension, increased nutrient, and Chl *a* concentrations was found to range from 2-7 days, and were consistent with results found in previous studies in this estuary (Morse et al., 2014; Egerton et al., 2014). I conclude that sediment resuspension appears to be another control on dinoflagellate blooms, shedding light on these persistent and complex phenomena.

Cultural eutrophication has long been linked with the formation of harmful algal blooms (Paerl, 1988; Smayda, 1990; Pinckney et al., 2001; Anderson et al., 2008). Due to the impacts nutrient-laden runoff can have on water quality, "green" infrastructure has been implemented along many waterways including, the Lafayette River (U.S. Environmental Protection Agency, 2015). The reduction of nutrient loading from runoff, via marsh restoration, living shorelines/bioretention cells and additional green infrastructure, reduce nutrient loading (Kemp et al., 2005; U.S. Environmental Protection Agency, 2015). However, based on the results of this study, it appears that the supply of nutrients from sediment resuspension can also fuel unwanted chlorophyll production, particularly in productive systems where excess organic matter can accumulate on the bottom where nutrients can be regenerated.

Sediment resuspension and its apparent effects on algal growth are likely to be exacerbated by the climate change. Many studies suggest climate change and sea level rise will lead to increases in harmful algal growth due to rising water temperatures, increased storm, flooding events, and loss of marsh (Kemp et al., 2005; Moore et al., 2008; Najjar et al., 2010).

Increased storm activity can result in increased sediment resuspension, which is likely to further amplify algal production via benthic-pelagic coupling.

Results from this study not only provide evidence that sediment resuspension can stimulate bloom initiation but also provides an important first step in developing and improving predictive models of bloom formation. In addition, it can be concluded that despite the importance of reducing surface nutrient runoff to mitigate the development of blooms and improve water quality, we also need to understand the role of sediment resuspension in re-introducing nutrients stored in the sediments to the water column where they can fuel algal growth. Future efforts to control blooms should also consider the location of cyst beds and factors that control germination cysts such as oxygen and nutrient concentrations. By better understanding how sediment resuspension effects the formation of dinoflagellate blooms, we can improve models and mitigation efforts to prevent them.

REFERENCES

Ahn, Y., Bricaud, A., & Morel, A. (1992). Light backscattering efficiency and related properties of some phytoplankters. *Deep Sea Research*, 1835-1855.

Allen, J. (1974). Reaction, relaxation and lag in natural sedimentaty systems: General principles, examples and lessons. *Earth-Science Reviews*, 263-342.

Anderson, D. M., Taylor, C. D., & Armbrust, E. (1987). The effects of darkness and anaerobiosis on dinoflagellate cyst germination. *Limnology and Oceanography*, 340-351.

Anderson, D., Burkholder, J., Cochlan, W., Gilbery, P., Gobler, C., Heil, C., . . . Vargo, G. (2008). Harmful algal blooms and eutrophication: Examining linkages from selected coastal regions of the United States. *Harmful Algae*, 39-53.

Arfi, R., Guiral, D., & Bouvy, M. (1993). Wind induced resuspension in a shallow tropical lagoon. *Estuarine, Coastal and Shelf Science*, 587-604.

Bale, A., Widdows, J., Harris, C., & Stephens, J. (2006). Measurements of the critical erosion threshold of surface sediments along the Tamar Estuary using mini-annular flume. *Continental Shelf Research*, 1206-1216.

Berman, M., Berquist, H., Hershner, C., Killeen, S., Rudnicky, T., Schatt, D., . . . Woods, H. (2002). *City of Norfolk- Shoreline situation report.* Applied Marine Science and Ocean Engineering.

Blair, C. H., Cox, J. H., & Kuo, C. Y. (1976). *Investigation of Flushing time in the Lafayette River, Norfolk, Virginia.* Norfolk: Old Dominion University Research Foundation.

Booth, J., Miller, R., McKee, B., & Leathers, R. (2000). Wind-induced bottom sediment resuspension in a microtidal coastal environment. *Continental Shelf Research*, 785-806.

Brand, A., Lacy, J. R., Hsu, K., Hoover, D., & Gladding, S. (2010). Wind-enhanced resuspension in the shallow waters of South San Francisco Bay: Mechanisms and potential implications for cohesive sediment transport. *Journal of Geophysical Research*.

Brown, L., Bresnan, E., Summerbell, K., & O'Neill, F. (2013). The influence of demersal trawl fishing gears on the resuspension of dinoflagellate cysts. *Marine Pollution Bulletin*, 17-24.

Butman, B., Aretxabaleta, A. L., Dickhudt, P. J., Dalyander, P. S., Sherwood, C. R., Anderson, D. M., . . . Signell, R. P. (2014). Investigationg the importance of sediment resuspension in Alexandrium fundyense cyst population dynamics in the Gulf of Maine. *Deep-Sea Research II*, 79-95.

Carniello, L., Defina, A., Fagherazzi, S., & D'Alpaos, L. (2005). A ombined wind wave-tidal model for the Venice lagoon, Italy. *Journal of Geophysical Research*.

Corbett, D. (2010). Resuspension and esturine nutrient cycling: insights from the Neuse River Estuary. *Biogeosciences*, 3289-3300.

de Jorge, V., & van Beusekom, J. (1995). Wind- and tide-induced resuspension of sediment and microphytobenthos from tidal flats in the Ems estuary. *Limnology and Oceanography*, 766-778.

Downing, J. (2006). Twenty-five years with OBS sensors: The good, the bad, and the ugly. *Continental Shelf Research*, 2299-2318.

Dwight, R., Caplan, J., Brinks, M., Catlin, S., Buescher, G., & Semenza, J. (2011). Influence of variable precipitation on coastal water quality in southern California. *Water Environment Research*, 2121-2130.

Egerton, T. A., Morse, R. E., Marshall, H. G., & Mulholland, M. R. (2014). Emergence of algal blooms: The effects of short-term variability in water quality on phytoplankton abundance, diversity, and community compsition in a tidal estuary. *Microorganisms*, 33-57.

Elfrink, B., Hanes, D. M., & Ruessink, B. (2006). Parameterization and simulation of near bed orbital velocities under irregular waves in shallow water. *Coastal Engineering*, 915-927.

Fagherazzi, S., Palermo, C., Rulli, M., Carniello, L., & Defina, A. (2007). Wind waves in shallow microtidal basins and the dynamic equilibrium of tidal flats. *Journal of Geophysical Research*.

Fanning, K., Carder, K., & Betzer, P. (1982). Sediment resuspension by coastal waters: A potential mechanism for nutrient recycling on the ocean's margins. *Deep-Sea Research*, 953-965.

Fenchel, T. (1992). What can ecologists learn from microbes: life beneath a square centimeter of sediment surface. *Functional Ecology*, 499-507.

Filippino, K., Egerton, T., Hunley, W., & Mulholland, M. (2017). The influences of storms on water quality and phytoplankton dynamics in the tidal James River. *Estuaries and Coasts*, 80-94.

Gartner, J. W. (2004). Estimating suspended solids concentrations from backscatter intensity measured by acoustic Doppler current profiler in San Francisco Bay, California. *Marine Geology*, 169-187.

Gibbons, D., Jones, G., Siegel, E., Hay, A., & Johnson, F. (1983). Performance of a new submersible tidal-wave recorded. *UNESCO Technical Paper in Marine Science*.

Gobbler, C. J., Berry, D. L., Anderson, O., Burson, A., Koch, F., Rodgers, B. S., . . . Nuzzi, R. (2008). Characterization, dynamics, and ecological impacts of harmful Cochlodinium plykrikoides blooms on eastern Long Island, NY, USA. *Harmful Algae*, 293-307.

Green, M. O., & Coco, G. (2013). Review of wave-driven sediment resuspension and transport in estuaries. *Reviews of Geophysics*, 77-117.

He, R., McGillicuddy, D., Anderson, D., & Keafer, B. (2008). Historic 2005 toxic bloom of Alexandrium fundyense in the western Gulf of Maine: 2. Coupled biophysical modellin. *Journal of Geophysical Research*.

Howarth, R., Swaney, D., Boyer, E., Marino, R., Jaworski, N., & Goodale, C. (2006). The influence of climate on average nitrogen export from large watersheds in the northeastern United States. *Biogeochemistry*, 163-186.

Jahnke, R., Alexander, C., & Kostka, J. (2003). Advective pore water input of nutrients to the Satilla River Estuary, Georgia, USA. *Esturine Coastal and Shelf Science*, 641-653.

Jeong, H., Yoo, Y., Lee, K., Kim, T., Seong, K., Kang, N., . . . Yih, W. (2013). Red tides in Masan Bay, Korea in 2004-2005: I. Daily variations in the abundance of red-tide organisms and environmental factors. *Harmful Algae*, S75-S88.

Keafer, B. A., Buesseler, K. O., & Anderson, D. M. (1992). Burial of living dinoflagellate cysts in estuarine and nearshore sediments. *Marine Micropalentology*, 147-161.

Kemp, W., & Boynton, W. (1996). Benthic-pelagic interactions: Nutrient and oxygen dynamics. In *Oxygen dynamics in the Chesapeake Bay* (pp. 149-221). College Park: Maryland Sea Grant.

Kemp, W., Boynton, W., Adolf, J., Boesch, D., Boicourt, W., Brush, G., . . . Stevenson, J. (2005). Eutrophication of Chesapeake Bay: historical trends and ecological interactions. *Marine Scology Progress Series*, 1-29.

Kremp, A. (2001). Effects of cyst resuspension on germination and seeding of two bloom-forming dinoflagellates in the Baltic Sea. *Marine Ecology Progress Series*, 57-66.

Kremp, A., & Anderson, D. (2000). Factors regulating germination of resting cysts of the spring bloom dinoflagellate Scrippsiella hangoei from the northern Baltic Sea. *Journal of Plankton Research*, 1311-1327.

Kremp, A., & Anderson, D. (2000). Factors regulating germination of resting cysts of the spring bloom dinoflagellate Scrippsiella hangoei from the northern Baltic Sea. *Journal of Plankton Research*, 1311-1327.

Kristensen, P., Sondergaard, M., & Jeppesen, E. (1992). Resuspension in a shallow eutrophic lake. *Hydrobiologia*, 101-109.

Lawson, S., Wiberg, P., McGlathery, K., & Fugate, D. (2007). Wind-Driver Sediment Suspension Controls Light Availabiality in a Shallow Coastal Lagoon. *Estuaries and Coasts*, 102-112.

Lee, D. (2008). Cochlodinium polykrikoides blooms and eco-physical conditions in the South Sea of Korea. *Harmful Algae*, 318-323.

Li, Z., Han, M., Matsuoka, K., Kim, S., & Shin, H. (2015). Identification of the resting cyst of Cochlodinium polykrikoides margalef (dinophyceae, gymnodiniales) in Korean coastal sediment. *Journal of Phycology*, 204-210.

Lim, A., Jeong, H., Jang, T., Kang, N., Jang, S., & Lee, M. (2015). Different effects of typhoons on ichthyotoxic Cochlodinium polykrikoides red tides in the South Sea of Korea during 2012-2014. *Harmful Algae*, 26-32.

Malvern Panalytical. (2018). *Laser Diffraction (LD)*. Retrieved from Malvern Panalytical: https://www.malvernpanalytical.com/en/products/technology/light-scattering/laser-diffraction

Margalef, R. (1961). Hidrografia y fitoplancton de un area marina de la costa meridional de Puerto Rico. *Investigacion Pesquera*, 76-78.

Matsuoka, K., Iwataki, M., & Kawami, H. (2008). Morphology and taxonomy of chain-forming species of the genus Cochlodinium (Dinophyceae). *Harmful Algae*, 261-270.

McGillicuddy, J., Townsend, D., He, R., Keafer, B., Kleindinst, J., Li, Y., . . . Anderson, D. (2011). Suppression of the 2010 Alexandrium fundyense bloom by changes in physical, biological, and chemical properties of the Gulf of Maine. *Limnology and Oceanography*, 2411-2426.

Mohamed, Z. A., & Al-Shehri, A. M. (2011). Occurance and germination of dinoflagellate cysts in surface sediments from the Red Sea off the coasts of Saudi Arabia. *OCEANOLOGIA*, 121-136.

Moore, S., Trainer, V., Mantua, N., Parker, M., Laws, E., Bracker, L., & Fleming, L. (2008). Impacts of climate variability and future climate change on harmful algal blooms and human health. *Environmental Health*.

Morse, R. E., Mulholland, M. R., Egerton, T. A., & Marshall, H. G. (2014). Phytoplankton and nutrient dynamics in a tidally dominated eutrohic estuary: daily variability and controls on bloom formation. *Marine Ecology*, 59-74.

Morse, R. E., Mulholland, M. R., Hunley, W. S., Fentress, S., Wiggins, M., & Blanco-Garcia, J. L. (2013). Controls on the iniation and development of blooms of the dinoflagellate Cochlodinium polykrikoides Margalef in Lower Chesapeake Bay and its tributaries. *Harmful Algae*, 71-82.

Morse, R. E., Shen, J., Blanco-Garcia, J. L., Hunley, W. S., Fentress, S., Wiggins, M., & Mulholland, M. R. (2011). Environmental and Physical Controls on the Formation and Transport of Bloos of the Dinoflagellate Cochlodinium polykrikoides Margalef in the Lower Chesapeake Bay and its Tributaries. *Estuaries and Coasts*, 1006-1025.

Mulholland, M. R., Morse, R. E., Boniello, G. E., Bernhardt, P. W., Filippino, K. C., Procise, L. A., . . . Gobler, C. (2009). Understanding causes and impacts of the dinoflagellate Cochlodinium polykrikoides, Blooms in the Chesapeake Bay. *Estuaries and Coasts*, 734-747.

Najjar, R. G., Pyke, C. R., Adams, M., Breitburg, D., Hershner, C., Kemp, M., . . . Wood, R. (2010). Potential climate-change impacts on the Chesapeake Bay. *Estuarine, Coastal and Shelf Science*, 1-20.

National Oceanic & Atmospheric Administration. (2018, August). *Climate at a Glance*. Retrieved from NOAA National Centers for Environmental Information: https://www.ncdc.noaa.gov/cag/city/rankings/USH00446139/pcp/201705

National Oceanic & Atmospheric Administration. (n.d.). *Meterological Observations*. Retrieved from NOAA Tides & Currents: https://tidesandcurrents.noaa.gov/map/index.shtml?type=active&region=Virginia

National Oceanic and Atmospheric Administration. (2018). *Data Access*. Retrieved from NOAA Naional Centers for Environmental Information: https://www.ncdc.noaa.gov/data-access

Nehring, S. (1996). Recruitment of planktonic dinoflagellates: Importance of benthic resting stages and resuspension events. *International Review of Hydrobiology*, 513-527.

Neumeier, U. (2003). *Processing of wave data from pressure sensors.* Retrieved from http://neumeier.perso.ch/matlab/waves.html

Nichols, M. M. (1992). Effects of fine sediment resuspension in estuaries. *Estuarine Cohesive Sediment Dynamics*, 5-42.

Ogston, A., & Sternberg, R. (1999). Sediment-transport events on the nothern California continental shelf. *Marine Geology*, 69-82.

Paerl, H. (1988). Nuisance phytoplankton blooms in coastal, esturine, and inland waters. *Limnology and Oceanography*, 823-847.

Paerl, H., Bales, J., Ausley, L., Buzzelli, C., Crowder, L., Eby, L., . . . Richardson, T. (2001). Ecosystem impacts of three sequential hurricanes (Dennis, Floyd, and Irene) on the United States' largest lagoonal estuary, Pamlico Sound, NC. *Proceedings of the National Academy of Sciences USA*, 5655-5660.

Pinckney, J., Paerl, H., Tester, P., & Richardson, T. (2001). The role of nutrient loading and eutrophication in esturine ecology. *Environmental Health Perspectives*, 699-706.

Pond, S., & Pickard, G. (1983). *Introductory Dynamical Oceanography.* New York: Pergamon Press Inc.

Rossi, L., Chevre, N., Fankhauser, R., Margot, J., Curdy, R., Babut, M., & Barry, D. (2013). Sediment contamination assessment in urban areas based on total suspended solids. *Water Research*, 339-350.

Schallenberg, M., & Burns, C. W. (2004). Effects of sediment resuspension on phytoplankton production: tesing apart the influences of light, nutrients, and algal entrainment. *Freshwater Biology*, 143-159.

Schoellhamer, D. (1993). Biological interference of optical backscatterance sensors in Tampa Bay, Florida. *Marine Geology*, 303-313.

Seaborn, D., & Marshall, H. (2008). Dinoflagellate cysts wihtin sediment collections from the southern Chesapeake Bay and tidal regions of the James, York, and Rappahannock rivers. *Virginia Journal of Science*, 135-141.

Shin, H., Li, Z., Yoon, Y., Oh, S., & Lim, W.-A. (2017). Formation and germination of temporary cysts of Cochlodinium polykrikoides Margalef (Dinophyceae) and their ecological role in dense blooms. *Harmful Algae*, 57-64.

Simon, N. (1988). Nitrogen cycling between sediment and the shallow-water column in the transitional zone of the Potomac River I. Nitrate and ammonium fluxes. *Esturine, Coastal, and Shelf Science*, 483-497.

Simon, N. (1989). Nitrogen cycling between sediment and the shallow-water column in the transitional zone of the Potomac River and Estuary. II. The role of wind-driven resuspension and adsorbed ammonium. *Esturine, Coastal, and Shelf Science*, 531-547.

Smayda, T. (1990). Novel and nuisance phytoplankton blooms in the sea: evidence for a global epidemic. In E. Graneli, B. Sunderstrom, L. Elder, & D. Anderson, *Toxic Marine Phytoplankton* (pp. 29-40). New York: Elsevier.

Smayda, T. (1997a). What is a bloom: A commentary. *Limnology and Oceanography*, 1132-1136.

Sondergaard, M., Kristensen, P., & Jeppesen, E. (1992). Phosphorus release from resuspended sediment in the shallow and wind-exposed Lake Arreso, Denmark. *Hydrobiologia*, 91-99.

Soulsby, R. (1983). Chapter 5: The bottom boundary layer of shelf seas. In B. Johns, *Physical oceanography of coastal and sheld seas* (pp. 189-266). Amsterdam: Elsevier Science Publishing Company.

Soulsby, R. (1997). *Dynamics of marine sands: A manual for practical applications.* London: Thomas Telford.

Stramski, D., & Kiefer, D. (1991). Light scattering by microorganisms in the open ocean. *Progress in Oceanography*, 343-383.

Tang, Y., & Gobler, C. J. (2012). The toxic dinoflagellate Cochlodinium polykrikoides (Dinophyceae) produces resting cysts. *Harmful Algae*, 71-80.

Tang, Y., Koch, F., & Gobler, C. (2010). Most harmful algal species are vitamin B1 and B12 auxotrophs. *Proceedings of the National Academy of Sciences*, 20756-20761.

Tango, P., Magnen, R., Butler, W., Luckett, C., Luckenbach, M., Lacouture, R., & Poukish, C. (2005). Impacts and potential effects due to Prorocentrum minimum blooms in Chesapeake Bay. *Harmful Algae*, 525-531.

Thoha, H., Muawanah, Bayu Intan, M., Rachman, A., Sianturi, O., Sidabutar, T., . . . Masseret, E. (2019). Resting cyst distribution and molecular identification of the harmful dinoflagellate Margalefidiniu polykrikoides (Gymnodiniales, Dinophyceae) in Lampung Bay, Sumatra, Indonesia. *Frontiers in Microbiology*.

U.S. Army Coastal Engineering Research Center (CERC). (1984). *Shore Protection Manual.* Fort Belvoir: U.S. Army Coastal Engineering Research Center .

U.S. Environmental Protection Agency. (1996). *Total maximum daily load (TMDL) program implementation strategy.* U.S. Environmental Protection Agency.

U.S. Environmental Protection Agency. (2015). *Restoring Knitting Mill Creek through Green Infrastructure.* Norfolk.

Virginia Institute of Marine Science. (2018). *City of Norfolk comprehensive map viewer*. Retrieved from Center for Coastal Resources Management: http://cmap2.vims.edu/CCRMP/Norfolk2014/Norfolk_CCRMP_Viewer.html

Webster, T., & Lemckert, C. (2002). Sediment resuspension within a microtidal estuary/embayment and the implication to channel management. *Journal of Coastal Research*, 753-759.

Wiberg, P. L., & Smith, J. D. (1987). Calculations of the critical shear stress for motion of uniform and heterogeneous sediments. *Water Resources Research*, 1471-1478.

You, Z.-J. (2005). Fine Sediment resuspension dynamics in a large semi-enclosed bay. *Ocean Engineering*, 1982-1993.

APPENDICES

APPENDIX A

Regression analysis results from bottom wave orbital velocity with near bed acoustic backscatter, SSC from the bottom OBS, and wind speed for deployments 3 and 6. Weak positive relationships appear to be present for deployment 3, and for wave orbital velocity vs wind speed for deployment 6.

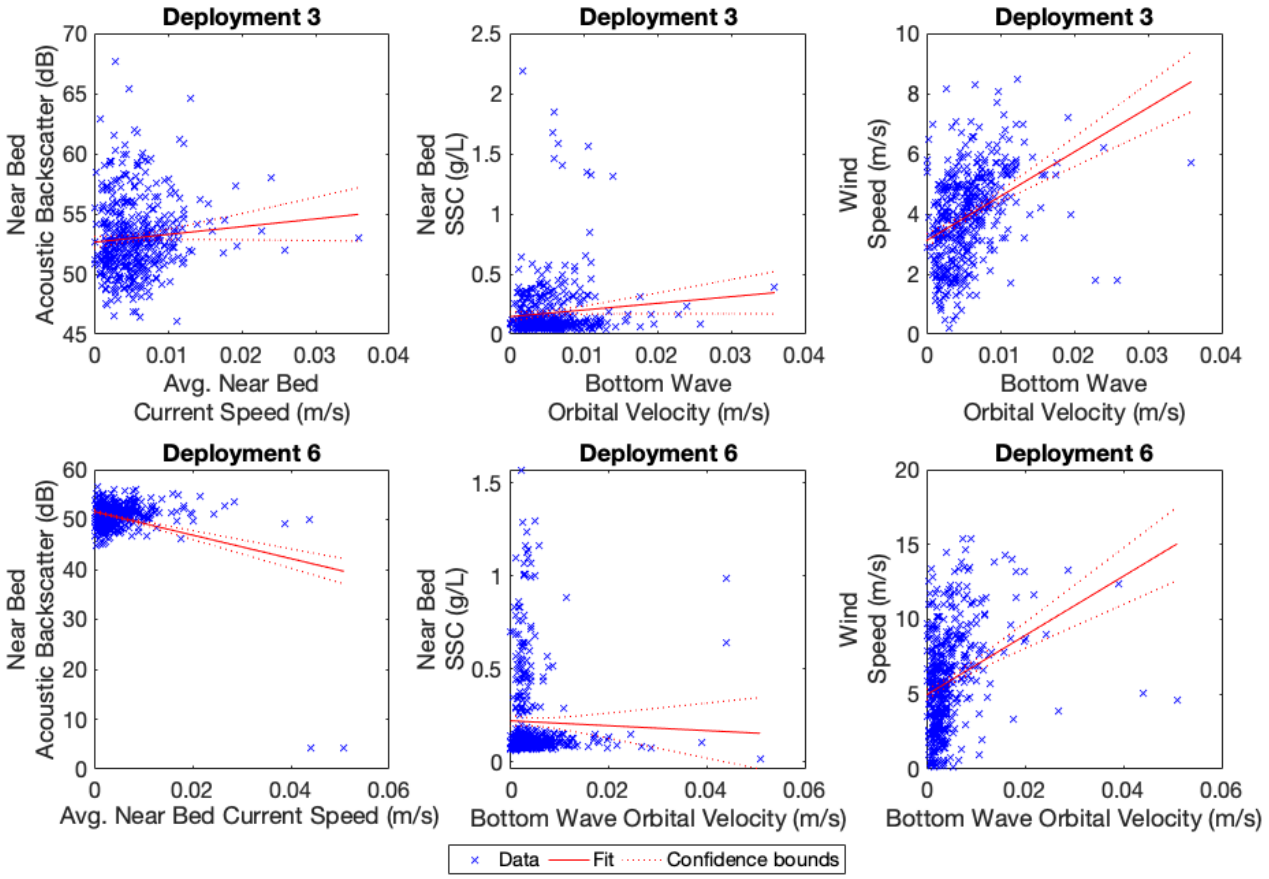

APPENDICES

APPENDIX B

Resulting R^2 and p-values from the regression analyses of near bed current speed and bottom wave orbital velocities with acoustic backscatter and SSC as well as bottom wave orbital velocity with acoustic backscatter, SSC, and wind speed.

	1	2	3	4	5	6
Current Spd x Acoustic Backscatter	**R^2=0.01 P-value < 0.05**	**R^2=-0.001 P-value =0.81**	**R^2=0.03 P-value < 0.05**	**R^2=0.078 P-value < 0.05**	**R^2=0.026 P-value < 0.05**	**R^2=0.01 P-value < 0.05**
Current Spd x Bottom OBS	**R^2=0.0034 P-value = 0.09**	**R^2=-0.001 P-value = 0.78**	**R^2=0.009 P-value < 0.05**	**R^2=0.0026 P-value =0.05**	**R^2=0.0003 P-value = 0.4**	**R^2=0-.002 P-value = 0.8**
Wave Orb. Vel x Acoustic Backscatter			**R^2=0.006 P-value = 0.09**			**R^2=0.13 P-value < 0.05**
Wave Orb Vel x Bottom OBS			**R^2=0.007 P-value < 0.05**			**R^2= - 0.001 P-value = 0.5**
Wave Orb. Vel x Wind Speed			**R^2=0.13 P-value < 0.05**			**R^2=0.1 P-value < 0.05**

APPENDIX C

Days that sediment resuspension events occurred, broken down by month between 5/7 and 10/1, categorized by approximate magnitude.

	0.5 g/L SSC < 1.5 g/L	1.5 g/L SSC 3 g/L	SSC 3 g/L
May	8, 10, 11, 12, 16, 24,	27, 30	None
June	1, 2, 3, 10, 12-14, 15, 17, 23, 30	18, 22, 24, 26-27, 28	20, 25
July	1, 3, 8, 16, 25, 27, 28	2, 4, 7, 10, 14, 17, 18	5, 6
August	1, 4, 6, 7, 8, 9, 10, 11, 19, 22, 24, 26	20, 23, 25, 27, 28, 29	None
Sept./Oct.	26, 28, 29, 30, 1	29	None

APPENDICES

APPENDIX D

Top panel- Scaled wind velocity for deployments 3-6. Middle panel- bottom averaged current speed (m/s) for deployments (colored lines), wave orbital velocity for deployments 3 and 6 (black lines). Bottom panel-near bed SSC (g/L) recorded by the bottom OBS.

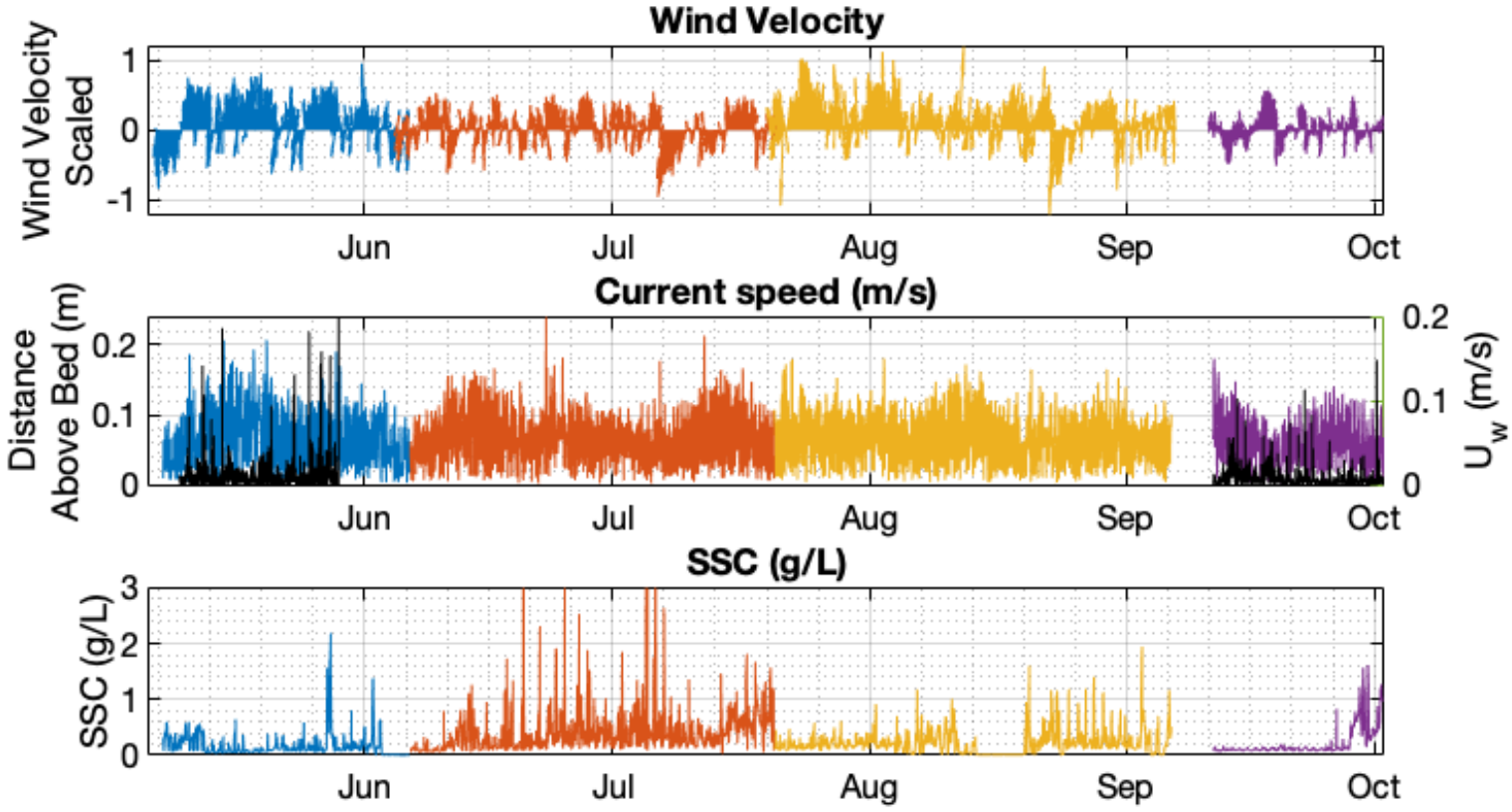

APPENDICES

APPENDIX E

Top panel: Scaled wind velocity and rainfall total. Second panel: Current speed. Third panel: Acoustic backscatter and near bed SSC (g/L) recorded by the bottom OBS, showing resuspension events. The red lines represent the 0.5 g/L and 1.5 g/L resuspension thresholds. Fourth panel: Bottom nutrient concentrations. Bottom panel: Chlorophyll a concentrations from multi depth water sample analysis.

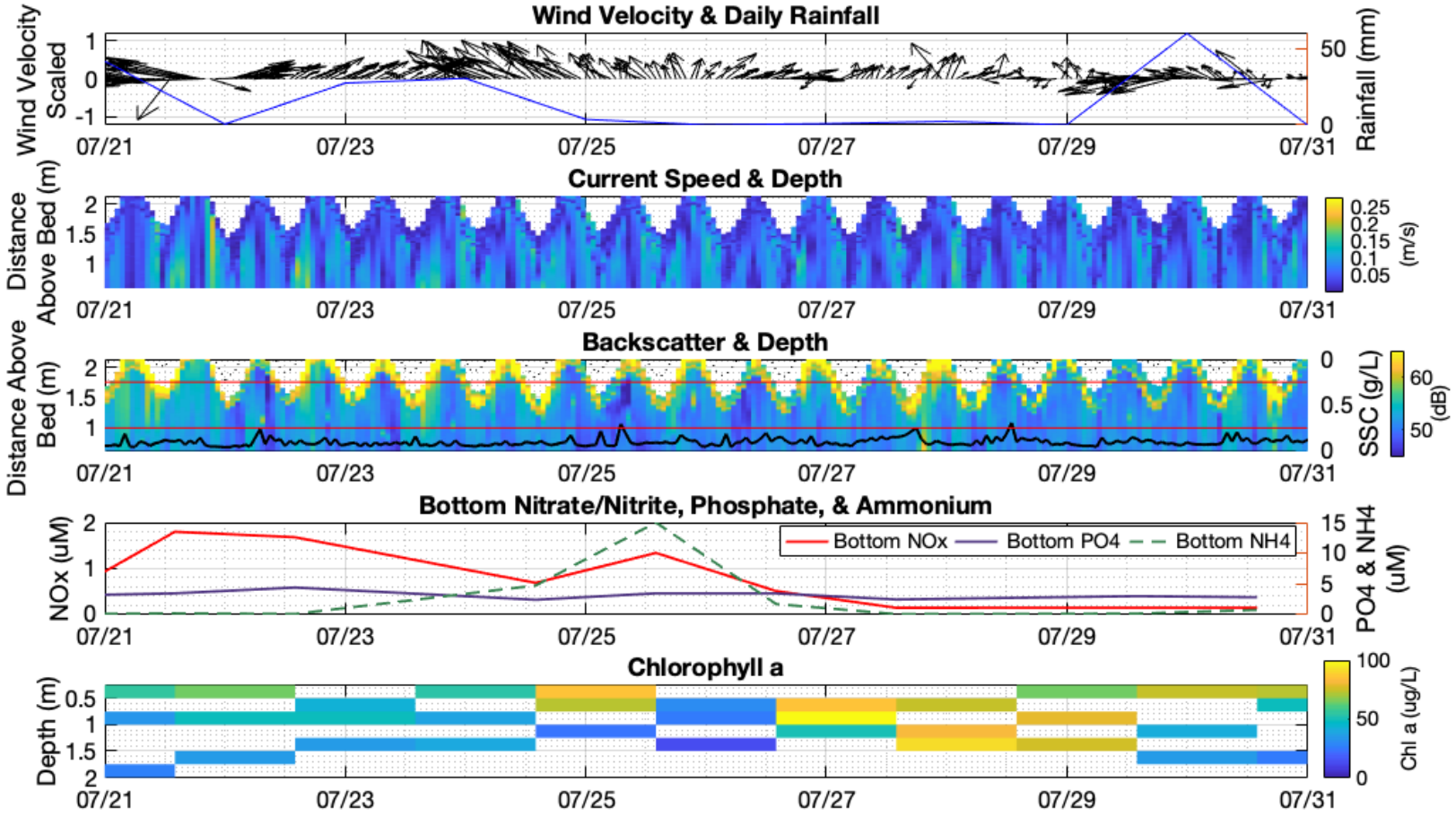

APPENDICES

APPENDIX F

Top panel: Scaled wind velocity and wind speed. Second panel: Acoustic backscatter and near bed SSC (g/L) recorded by the bottom OBS (solid black line), showing resuspension events. The red lines represent the 0.5 g/L and 1.5 g/L resuspension thresholds. Third panel:, Surface Chl a and Chl a with a filter to remove any tidal signal. Bottom panel: Bottom current speed and daily rainfall totals.

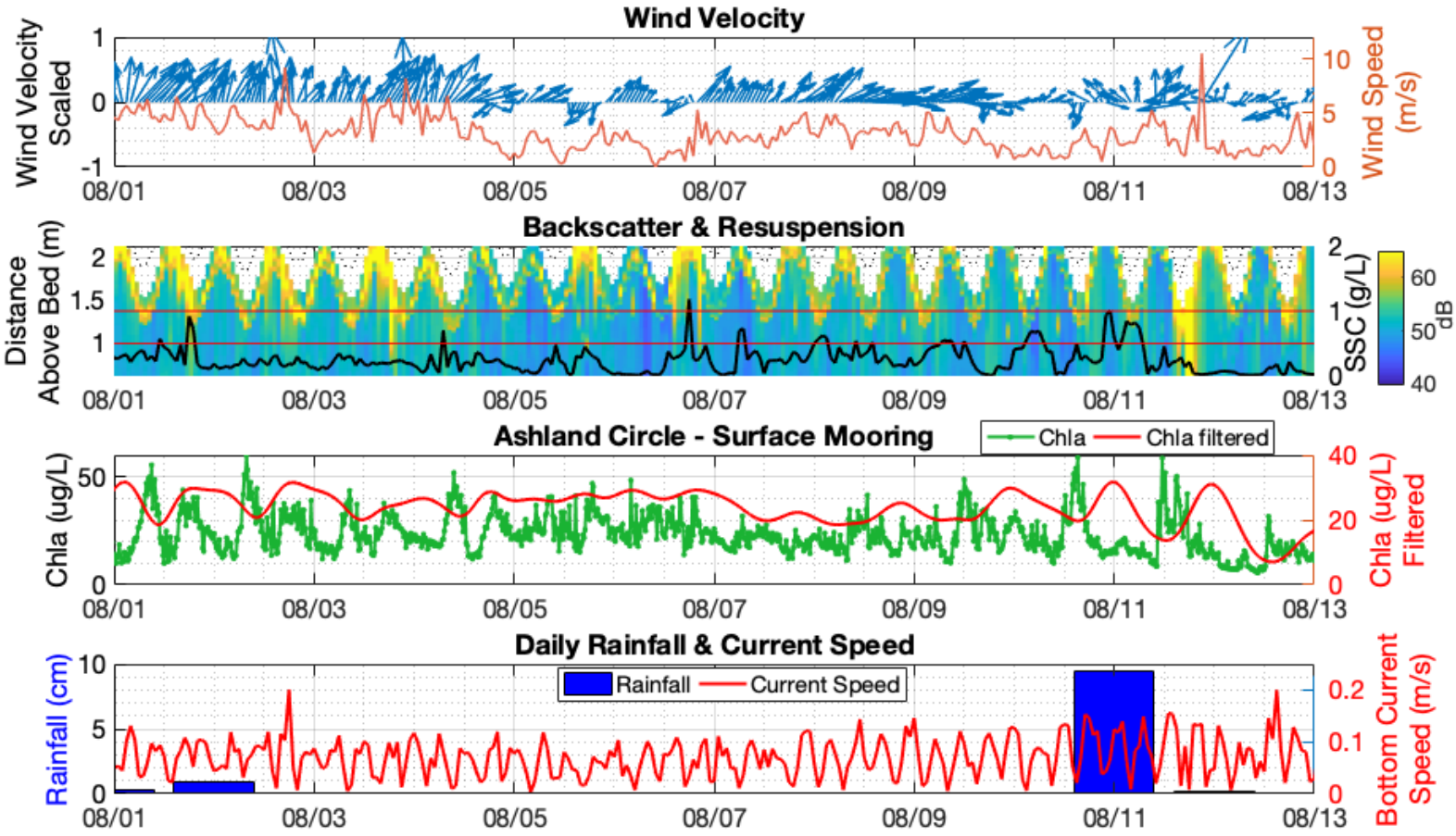

APPENDICES

APPENDIX G

Top panel: Scaled wind velocity and wind speed. Second panel: Acoustic backscatter and near bed SSC (g/L) recorded by the bottom OBS (solid black line) and top OBS (dashed line), showing resuspension events. The red lines represent the 0.5 g/L and 1.5g/L resuspension thresholds. Third panel: Surface Chl a and Chl a with a filter to remove any tidal signal. Bottom panel: Bottom current speed and daily rainfall totals

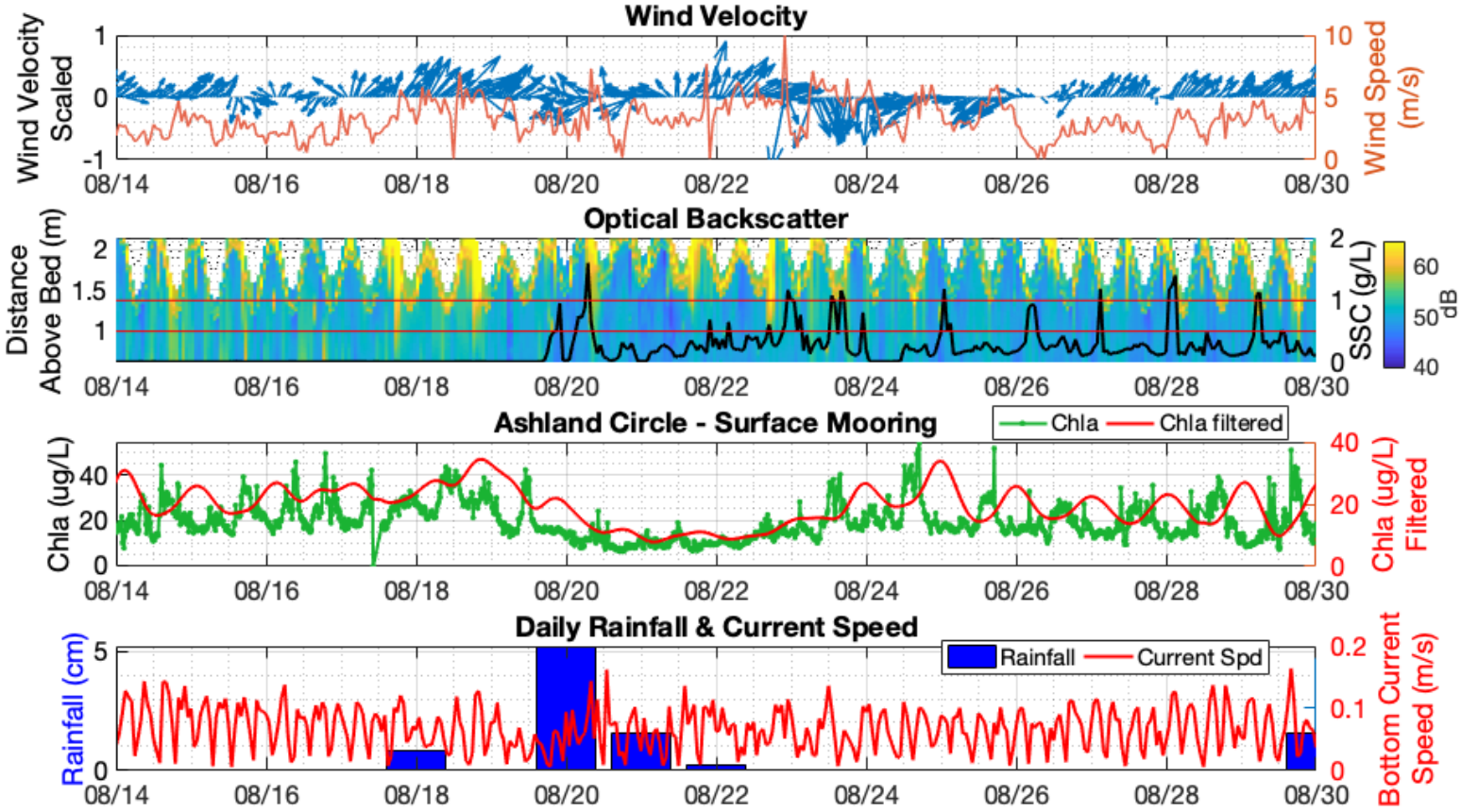

APPENDICES

APPENDIX H

Suspended sediment concentrations estimated from the calibrated bottom OBS' for each deployment were plotted against backscatter intensity recorded by the ADCP.

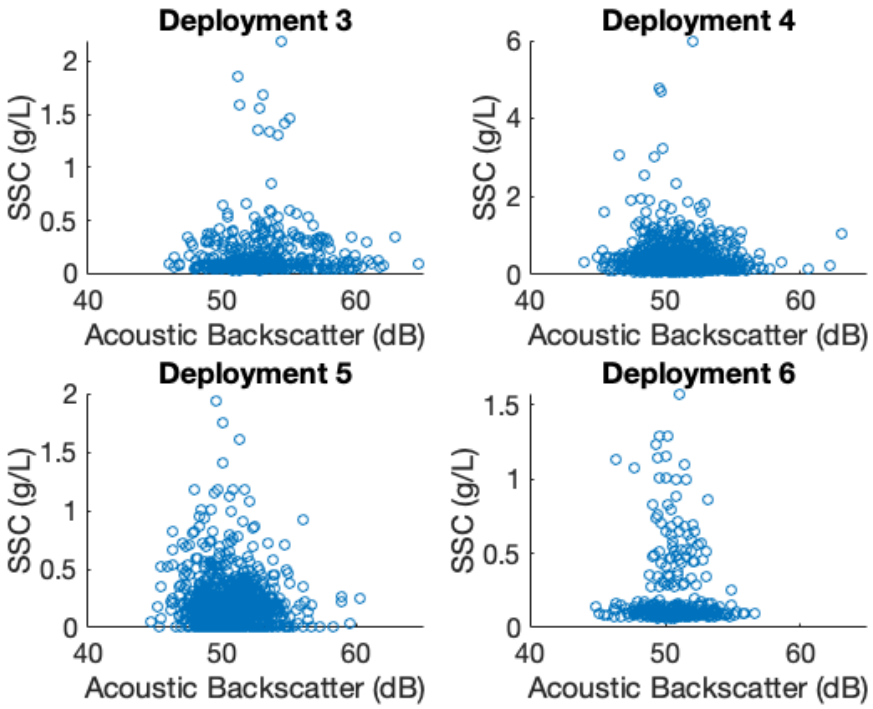

APPENDICES

APPENDIX I

Wind Roses which display the frequency of wind speed and direction for deployments 1 and 2. The seasonal wind patterns show weak southerly/southwesterly winds during that start mid spring and end early Fall. While strong Northeasterly or Northerly winds are more frequent Starting Early Fall into Spring.

Deployment 1: 1/26-2/19

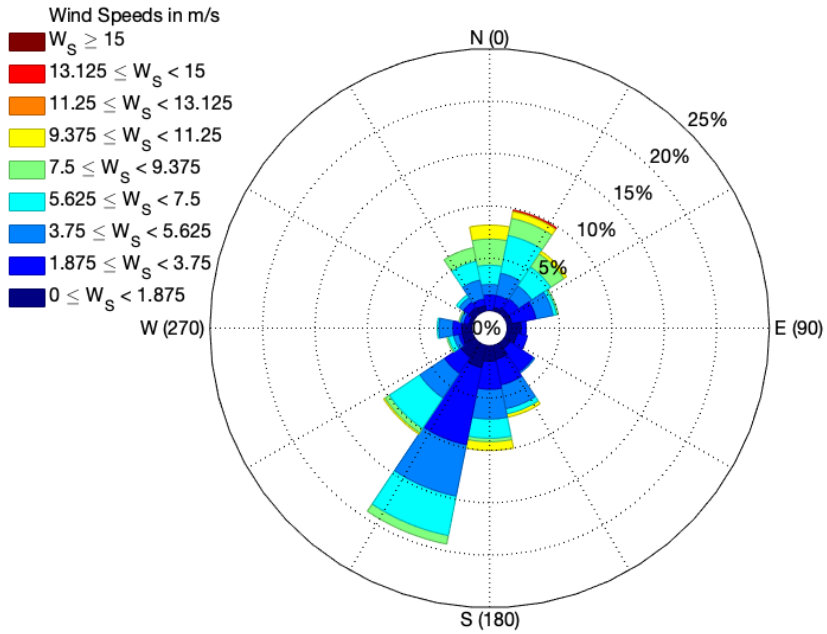

Deployment 2: 4/2-5/7

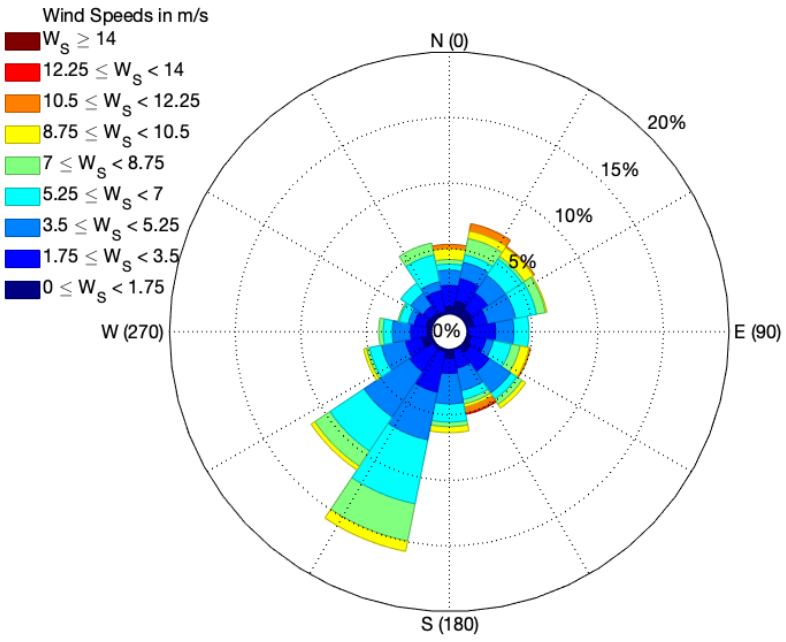

APPENDICES

APPENDIX J

Wind Roses which display the frequency of wind speed and direction for deployments 3 and 4. The seasonal wind patterns show weak southerly/southwesterly winds during that start mid spring and end early Fall. While strong Northeasterly or Northerly winds are more frequent Starting Early Fall into Spring.

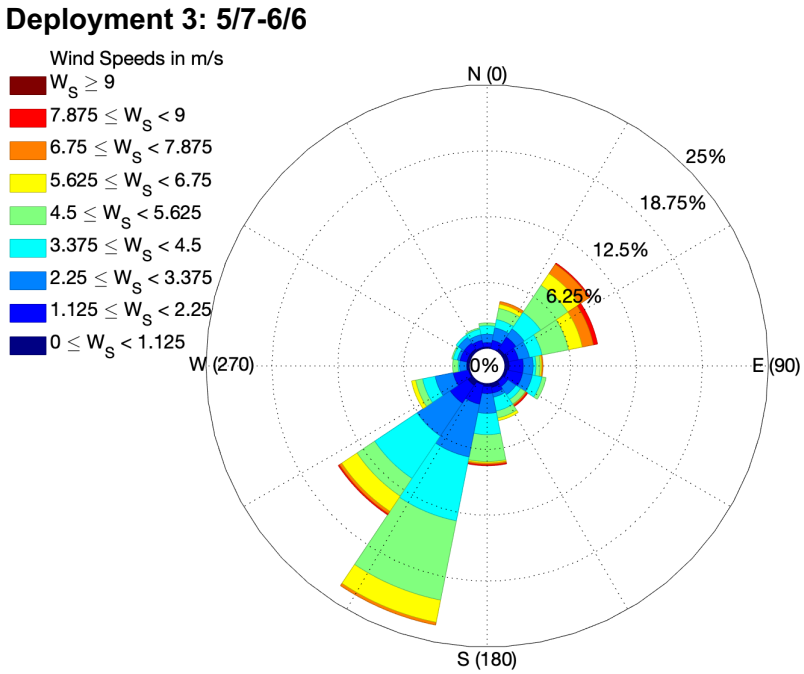

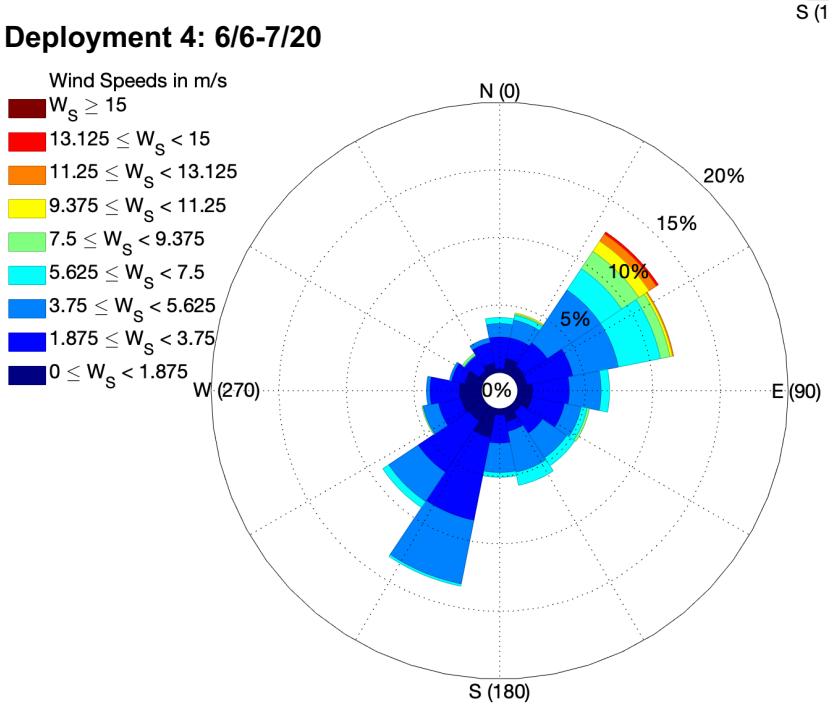

APPENDICES

APPENDIX K

Wind Roses which display the frequency of wind speed and direction for deployments 5 and 6. The seasonal wind patterns show weak southerly/southwesterly winds during that start mid spring and end early Fall. While strong Northeasterly or Northerly winds are more frequent Starting Early Fall into Spring.

Deployment 5: 7/20-9/6

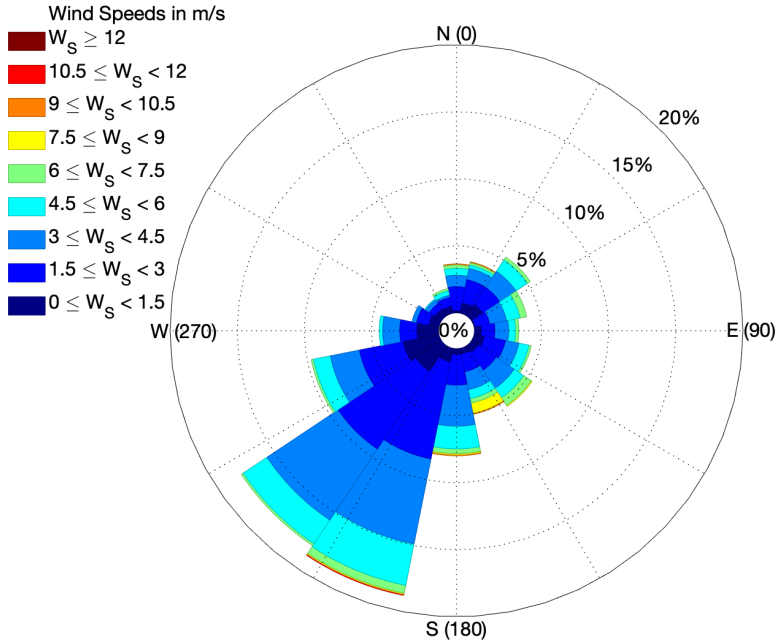

Deployment 6: 9/11-10/2

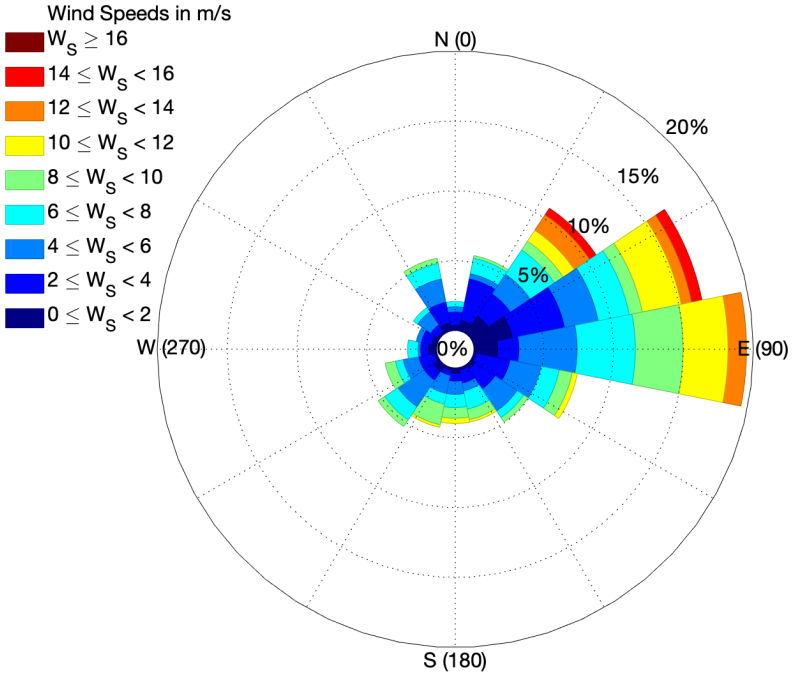

APPENDICES

APPENDIX L

Wind Roses which display the frequency of wind speed and direction for all of 2018. The seasonal wind patterns show weak southerly/southwesterly winds during that start mid spring and end early Fall. While strong Northeasterly or Northerly winds are more frequent Starting Early Fall into Spring.

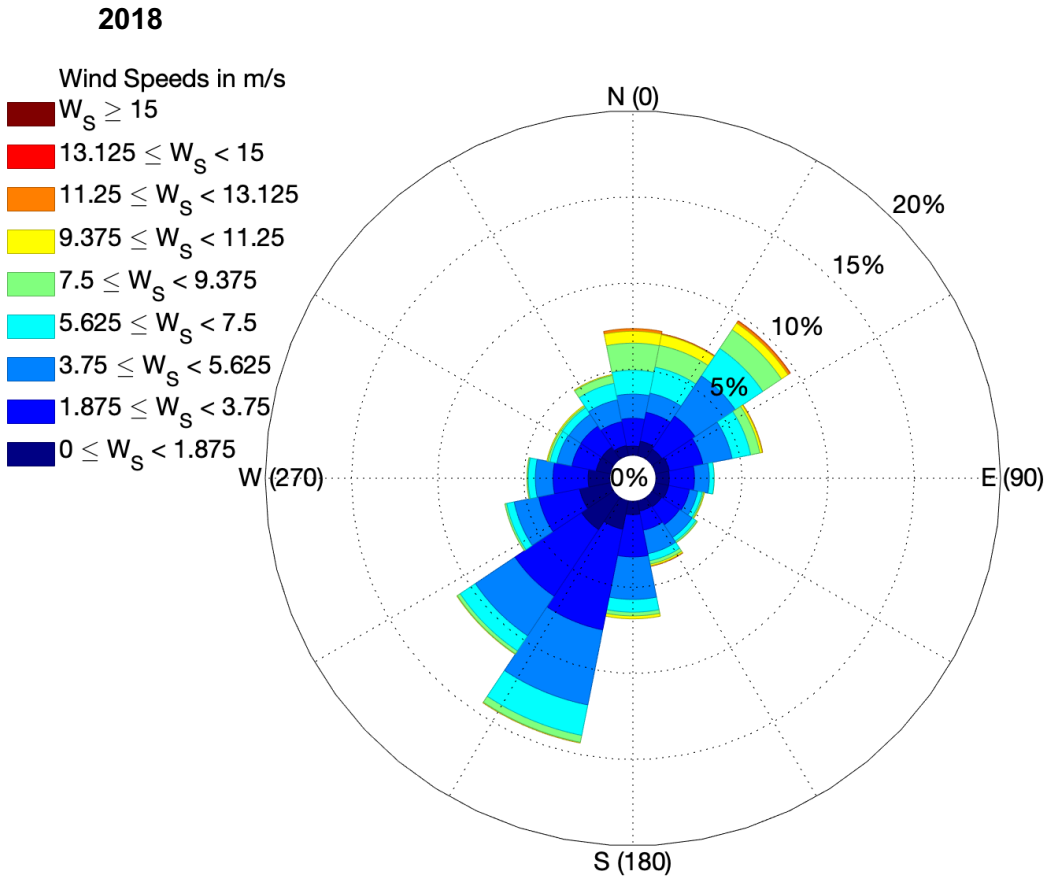

VITA

Samantha C. McGill

Old Dominion University
Department of Ocean, Earth, and Atmospheric Sciences
4600 Elkhorn Avenue, Norfolk, VA 23529 USA

EDUCATION

Master of Science — Ocean and Earth Sciences
Old Dominion University — G.I.S. Certificate
Norfolk, VA | 2019

Thesis**: Sediment Resuspension in a Microtidal Estuary: Causative Forces and Links with Algal Blooms**

Bachelor of Science: — Marine Science
Coastal Carolina University — Biology Minor
Conway, SC | 2013 — Environmental Science Minor

PUBLICATION

McGill, S.C., and Hale, R.P. An Investigation of Sediment Resuspension's Role in the Proliferation of Harmful Algal Blooms. *In Prep: Estuarine, Coastal, and Shelf Science*

PRESENTATIONS

McGill, S.C., and Hale, R.P. An Investigation of Sediment Resuspension's Role in the Proliferation of Harmful Algal Blooms. Southeast GSA Meeting, Charleston SC. March 2019.

McGill, S.C., Hale, R.P., and Mulholland, M. Sediment resuspension and its possible link to harmful algal blooms in a shallow micro-tidal estuary. AGU Fall Meeting, Washington, DC. December 2018.

Hale, R.P., Brown, K.F., and **McGill, S.C.** Sediment Dynamics of the Lower James River, VA. Southeast GSA Meeting, Charleston SC. March 2019.